1

NASA TECHNICAL MEMORANDUM 104076
AVSCOM TECHNICAL REPORT 91-B-011

LOCAL DELAMINATION IN LAMINATES WITH ANGLE PLY MATRIX CRACKS: PART II DELAMINATION FRACTURE ANALYSIS AND FATIGUE CHARACTERIZATION

T. K. O'Brien

Paper Presented at the 4th ASTM Conference on Composite Materials: Fatigue and Fracture Indianapolis, Indiana May 6-7, 1991

JUNE 1991

NASA

National Aeronautics and Space Administration

Langley Research Center
Hampton, Virginia 23665

92

SUMMARY

Constant amplitude tension-tension fatigue tests were conducted on AS4/3501-6 graphite epoxy $(0_2/\theta_2/-\theta_2)_s$ laminates, where θ was 15, 20, 25, or 30 degrees. Fatigue tests were conducted at a frequency of 5 Hz and an R-ratio of 0.1. Dye penetrant enhanced X-radiography was used to document the onset of matrix cracking in the central $-\theta$ degree plies, and the subsequent onset of local delaminations in the $\theta/-\theta$ interface at the intersection of the matrix cracks and the free edge, as a function of the number of fatigue cycles.

Two strain energy release rate solutions for local delamination from matrix cracks were derived: one for a local delamination growing from an angle ply matrix crack with a uniform delamination front across the laminate width, and one for a local delamination growing from an angle ply matrix crack with a triangular shaped delamination area that extended only partially into the laminate width from the free edge. Plots of G_{max} vs. N were generated to assess the accuracy of these G solutions. The influence of residual thermal and moisture stresses on G were also quantified. However, a detailed analysis of the G components and a mixed-mode fatigue failure criterion for this material may be needed to predict the fatigue behavior of these laminates.

INTRODUCTION

In part I of this study [1], the damage observed in quasi-static tension tests on $(0_2/\theta_2/-\theta_2)_s$ AS4/3501-6 graphite/epoxy laminates, where θ was 15, 20, 25, and 30 degrees, was documented. In addition, the stresses responsible for the matrix cracking and associated local delamination observed were calculated using finite element analyses.

In part II of this study, fatigue tests were conducted on $(0_2/\theta_2/-\theta_2)_s$ AS4/3501-6 graphite/epoxy laminates, where θ was 15, 20, 25, and 30 degrees. Constant amplitude, tension-tension fatigue tests were conducted at a frequency of 5 Hz and an R-ratio of 0.1. Dye penetrant enhanced X-ray radiography was used to document the onset of matrix cracking, and the subsequent onset of local delaminations at the intersection of the matrix cracks and the free edge, as a function of the number of fatigue cycles. Two strain energy release rate, G, solutions were introduced for local delamination from matrix cracks. These G solutions were used to correlate the onset of local delamination in fatigue between layups with different off-axis angle plies.

EXPERIMENTS

Materials

As documented in part I [1], panels were manufactured in an autoclave at NASA Langley Research Center from Hercules AS4/3501-6 graphite epoxy prepreg using the standard manufacturer's procedure with a maximum temperature of 177°C (350°F) in the cure cycle. One panel was produced for each of the $(0_2/\theta_2/-\theta_2)_s$ layups, where θ was 15, 20, 25, or 30 degrees. Panels 305 mm (12 in.) square were manufactured and then cut into 20 individual coupons, 127 mm (5.0 in.) long by 25 mm (1.0 in.) wide. Each specimen had a nominal ply thickness of 0.124 mm (0.0049 in.) and a fiber volume fraction of 67%.

Experimental Procedures

All static tests were conducted using the procedure outlined in part I of this study [1]. Fatigue specimens were placed in the hydraulic grips of a hydraulic load frame such that each specimen

had a gage length between the grips of approximately 76 mm (3.0 inches). A 25 mm (one inch) gage length extensometer was mounted on the specimen midway between the grips to measure nominal strain. As specimens were loaded quasi-statically to the mean load, a plot of load versus nominal strain was generated using an X-Y recorder. The extensometer was then removed, and the specimens were loaded at a cyclic frequency of 5Hz and an R-ratio of 0.1. Tests were run at several maximum load levels below the critical load required to initiate damage in the static tests. The cyclic loading was stopped at fixed cyclic intervals and a zinc iodide solution that was opaque to X-rays was placed on the edge using a hypodermic needle. A radiograph was taken of the specimen width, with the specimen loaded at the mean load, to document the presence of matrix cracking and delamination.

Table 1 lists the maximum cyclic loads and the schedule used to obtain radiographs for each cyclic load level. For example, tests run at maximum cyclic loads of 5000 and 6000 pounds were interrupted every 1000 cycles to obtain a radiograph of the specimen. Tests run at a maximum cyclic load of 3500 lbs were interrupted every 1000 cycles for the first 10,000 cycles; every 2,000 cycles between 10,000 and 20,000 cycles; every 5,000 cycles between 20,000 and 50,000 cycles; and every 10,000 cycles thereafter, to obtain a radiograph of the specimen. Loading was continued until a radiograph clearly indicated the presence of a local delamination associated with a matrix crack near the free edge. After the fatigue specimens were removed from the hydraulic grips, the edges were polished and examined in the light microscope. Photographs of the polished edges were taken through an optical microscope to document the damage observed on the straight edge.

Initially, some coupons were coated with a thin film of water-based typewriter correction fluid on either edge. After a few fatigue tests were performed, however, it was apparent that the onset of matrix cracking and local delamination was difficult to detect visually on the edge with this brittle coating. Hence, most of the fatigue coupons were tested without coating the edges. It was also easier to see the formation of the matrix cracks in the radiographs if there was no coating on the edge, because the dye penetrant used to reveal the damage was more likely to accumulate near a coated edge.

Experimental Results

Static Tests

The results from the quasi-static tests were documented in part I of this study [1]. The radiographs showed triangular-shaped shaded regions bounded by the free edge and matrix cracks, indicating that a local delamination was present. Edge micrographs showed that local delaminations were present in both $\theta/-\theta$ interfaces, extending in the same direction from curved matrix cracks in the central $-\theta$ degree plies.

Fatigue Tests

The same type of damage seen in the radiographs and edge micrographs of specimens taken after the quasi-static tests was present in the specimens that were tested in fatigue [1]. However, unlike the quasi-static tests, the sequence of damage was evident in the series of radiographs taken during the cyclic loading. For example, fig. 1 shows radiographs taken immediately after the onset of matrix cracking (fig.1a), and the subsequent onset of local delamination from the matrix crack (fig.1b), for a $(0_2/20_2/-20_2)_s$ laminate that was subjected to a maximum cyclic load of 15,570 N (3500 lbs). Similar radiographs were obtained for the other layups tested in fatigue. At the number of cycles corresponding to local delamination onset, all of the specimens had at least one, and in most cases, several matrix cracks in the central $-\theta$ degree plies. A few matrix cracks were also observed in the $+\theta$ degree plies for some laminates. Table 2 lists the average number of matrix cracks in the gage section measured from the radiographs of laminates taken just after the onset of local delamination. Local delaminations were present in the $\theta/-\theta$ interfaces near some, but not all, of these matrix cracks. By the time the fatigue tests were terminated, matrix cracks had also developed in the $+\theta$ degree plies of many laminates. Delaminations in the $\theta/-\theta$ interfaces often terminated at these $+\theta$ degree matrix ply cracks (fig.2).

Figures 3-6 show the cumulative number of cycles to the onset of matrix cracking and subsequent local delamination onset for each layup. The load at onset of damage (matrix cracking and local delamination) under a monotonically increasing load, determined in part I of this study, is shown on the ordinate. Figures 7-10 show the

cumulative number of cycles to local delamination onset minus the number of cycles to onset of matrix cracking. Hence, figures 7-10 represent the number of cycles to delamination onset once the matrix crack is present.

STRAIN ENERGY RELEASE RATE ANALYSIS

Uniform Local Delamination

In reference [2], an equation was derived for the strain energy release rate associated with a uniform local delamination growing from a 90 degree matrix crack (fig.11a) in a multidirectional laminate using the classical definition for G as

$$G = \frac{P^2}{2}\frac{dC}{dA} \qquad (1)$$

where dC is the incremental change in laminate compliance associated with an incremental change in surface area, dA, created by the local delamination. This solution assumed that the composite consisted of a laminated region and a locally delaminated region in series, resulting in the following expression

$$G = \frac{P^2}{2mw^2}\left(\frac{1}{t_{LD}E_{LD}} - \frac{1}{tE_{LAM}}\right) \qquad (2)$$

where P is the applied mechanical load on the laminate, w is the laminate width, and m is the number of delaminations growing from the matrix crack. The parameter, m, would have a value of 2 if the cracked off-axis ply is in the interior of the laminate, corresponding to local delamination on either side of the matrix crack. However, m would have a value of 1 if the cracked off-axis ply was a surface ply. In eq(2), t is the laminate thickness, E_{LAM} is the laminate modulus (as calculated from laminated plate theory), t_{LD} is the thickness of the locally delaminated region that carries the load (i.e., the laminate thickness minus the thickness of the cracked off-axis plies), and E_{LD} is the modulus of the locally delaminated region (as calculated from laminated plate theory).

As shown in appendix 1, eq(2) also applies to the case of a uniform delamination growing from an angle ply matrix crack as shown in fig.(11b). For the laminates in this study, t = Nh and t_{LD} = (N-n)h, where N is the number of plies in the laminate, n is the

number of cracked off-axis plies, and h is the ply thickness. Therefore, noting that $N_x = P/w$, eq(2) may be rewritten as

$$G = \frac{N_x^2}{2mh}\left(\frac{1}{(N-n)E_{LD}} - \frac{1}{NE_{LAM}}\right) \qquad (3)$$

The twelve-ply $(0_2/\theta_2/-\theta_2)_s$ laminates tested in this study may be analyzed as six-ply laminates with twice the measured ply thickness. Hence, N=6, n=2, and N-n=4. Then, noting that m=2 for an interior $-\theta$ matrix ply crack, a normalized strain energy release rate may be calculated as

$$\frac{Gh}{N_x^2} = \frac{1}{4}\left(\frac{1}{4E_{LD}} - \frac{1}{6E_{LAM}}\right) \qquad (4)$$

Bending-Extension Coupling Influence on G

The value of E_{LD} in eq.(4) depends on whether or not the locally delaminated region consists of symmetric or asymmetric sublaminates. For example, the locally delaminated region may be thought of as a $(0/\theta)_s$ symmetric sublaminate. In this case, the modulus of the locally delaminated region is simply

$$E_{LD} = \frac{1}{(N-n)h(A_{11})^{-1}} \qquad (5)$$

where $(A_{11})^{-1}$ is the first term of the inverse extensional stiffness matrix for the $(0/\theta)_s$ sublaminate. However, as noted in ref. [3], if the locally delaminated region consists of two 2-ply asymmetric sublaminates, then the presence of bending-extension coupling should be reflected in the modulus calculation. This may be accomplished using laminated plate theory by prescribing an applied mechanical strain, ε_x, setting the applied N_y, N_{xy}, and M_y equal to 0, and setting κ_x and κ_{xy} equal to 0. The N_x that results from this analysis is derived in appendix 2 and may be used to determine E_{LD} as

$$E_{LD} = \frac{2}{(N-n)h}\left[A_{11} + \left(\frac{D_1}{D}\right)A_{12} + \left(\frac{D_2}{D}\right)A_{16} + \left(\frac{D_3}{D}\right)B_{12}\right] \qquad (6)$$

where D_1, D_2, D_3, and D are functions of various terms in the A, B, and D matrices as defined in appendix 2.

Any difference between equations 5 and 6 reflects the constraint imposed on the 2-ply asymmetric sublaminate by the undamaged laminate and the grips (if the sublaminate extends into the grips). Because of this constraint, the sublaminate is not able to develop a κ_x or κ_{xy} curvature. However, under tension loading, a non-zero κ_y curvature may develop away from the grips in the sublaminate. For the type of sublaminates that form as a result of edge delamination [3-5], this influence of bending-extension coupling may be significant. However, for the $(0/\theta)_T$ sublaminates that constitute the locally delaminated region in the $(0/\theta/-\theta)_S$ laminates with $-\theta$ matrix cracks, the influence of bending-extension coupling is small. This small influence is shown in fig.12, where the normalized G of eq(4) is calculated as a function of θ for $(0/\theta/-\theta)_S$ laminates with $-\theta$ matrix cracks using material properties in Table 3. The normalized G values determined by calculating E_{LD} from eq(5) assuming a symmetric $(0/\theta)_S$ sublaminate are nearly identical to the normalized G values determined by calculating E_{LD} from eq(6) using the loading prescribed above in the laminated plate theory analysis. However, unlike many of the sublaminates formed by edge delamination, the $(0/\theta)_T$ sublaminates that constitute the locally delaminated region in the $(0/\theta/-\theta)_S$ laminates with $-\theta$ matrix cracks will also exhibit shear-extension coupling. This shear-extension coupling may have more influence on the calculated E_{LD} than the bending extension coupling.

Shear-Extension Coupling Influence on G

The influence of shear-extension coupling on the calculated E_{LD} for the 2-ply asymmetric sublaminate may be determined using laminated plate theory by prescribing the loading outlined above, but setting $\gamma_{xy} = 0$ instead of prescribing $N_{xy} = 0$. The N_x that results from this analysis is derived in appendix 2 and may be used to determine E_{LD} as

$$E_{LD} = \frac{2}{(N-n)h}\left[A_{11} - \left(\frac{A_{12}D_{22} - B_{12}B_{22}}{A_{22}D_{22} - B_{22}B_{22}}\right)A_{12} + \left(\frac{A_{12}B_{22} - A_{22}B_{12}}{A_{22}D_{22} - B_{22}B_{22}}\right)B_{12}\right] \qquad (7)$$

This E_{LD} value reflects the shear constraint imposed on the locally delaminated region by the undamaged laminated region. The shear constraint results in a greater apparent stiffness, E_{LD}, and hence, a correspondingly lower strain energy release rate. Figure 12 shows the normalized G of eq(4), calculated as a function of θ for $(0/\theta/-\theta)_S$ laminates with $-\theta$ matrix cracks, where the normalized G values were determined by calculating E_{LD} using eq(7). This loading assumes that the locally delaminated region consists of two 2-ply $(0/\theta)_T$ asymmetric sublaminates with bending-extension and shear-extension coupling. As shown in fig.12, the normalized G values determined by calculating E_{LD} using eq(7) are significantly lower than the normalized G values determined by calculating E_{LD} using eqs(5&6) for θ between 15 and 30 degrees.

Uniform Local Delamination vs. Edge Delamination

As noted earlier, the delaminations that form in the $\theta/-\theta$ interfaces of $(0/\theta/-\theta)_S$ laminates are localized and bounded by $-\theta$ degree ply matrix cracks. Hence, the physical evidence dictates that these delaminations should be analyzed as local delaminations. However, it may be enlightening to calculate the strain energy release rate, G, for edge delamination in the $\theta/-\theta$ interfaces of the $(0/\theta/-\theta)_S$ laminates and compare that to the corresponding G for local delamination. The strain energy release rate, G, for edge delamination is given by [4]

$$G = \frac{\varepsilon^2 t}{2}\left(E_{LAM} - E^*\right) \qquad (8)$$

where ε is the nominal applied strain, t is the laminate thickness, E_{LAM} is the laminate modulus, and E^* is the modulus of the laminate once it is totally delaminated, as determined by the rule of mixtures

$$E^* = \frac{\sum_{i=1}^{M} E_i t_i}{t} \qquad (9)$$

where M is the number of sublaminates formed by the edge delamination and E_i and t_i are the modulus and thickness of the i

sublaminates, respectively. For edge delamination in the θ/-θ interfaces of the $(0/\theta/-\theta)_s$ laminates, eq(9) becomes

$$E^* = \frac{2E_{(0/\theta)} + E_{(-\theta)}}{3} \qquad (10)$$

The strain energy release rate calculated in eq(8) will depend on the assumptions used to determine the (0/θ) and (-θ) sublaminate moduli in eq(10), which determines the delaminated modulus, E^*, in eq(9).

To compare the different possibilities, eq(8) was rearranged to yield a normalized G as

$$\frac{G}{\varepsilon^2 t} = \frac{1}{2}(E_{LAM} - E^*) \qquad (11)$$

Figure 13 shows the normalized strain energy release rate, $G/\varepsilon^2 t$, for edge delamination in the θ/-θ interfaces of the $(0/\theta/-\theta)_s$ laminates as a function of θ where the sublaminate moduli were determined assuming they were either symmetric, asymmetric with bending-extension coupling only (B/E Coupling), or asymmetric with shear-extension coupling in addition to bending-extension coupling (B/E & S/E Coupling). Unlike the comparison for local delamination, there is a significant difference in the normalized G for edge delamination between the symmetric sublaminate case and the bending-extension coupling case. This difference results from the effect of bending-extension coupling on the modulus of the -θ sublaminate in eq(10) which does not contribute to G for local delamination. Furthermore, when the influence of shear-extension coupling is included, the normalized G for edge delamination becomes very small for all values of θ.

In order to compare normalized G values for both local and edge delamination, Hooke's law in the form $N_x = Nh\varepsilon E_{LAM}$, where N=6, was substituted into eq(4) to yield

$$\frac{G}{\varepsilon^2 t} = \frac{3E_{LAM}^2}{2}\left(\frac{1}{4E_{LD}} - \frac{1}{6E_{LAM}}\right) \qquad (12)$$

Figure 14 shows G normalized by $\varepsilon^2 t$ for edge delamination and uniform local delamination, as calculated by eqs.(11) and (12)

respectively, as a function of θ for delamination in the $\theta/-\theta$ interfaces of the $(0/\theta/-\theta)_s$ laminates. The sublaminate moduli were determined assuming they were asymmetric, with shear-extension coupling in addition to bending-extension coupling. Figure 14 indicates that, for the same applied strain, the strain energy release rate associated with a uniform local delamination from a matrix crack exceeds the strain energy release rate associated with edge delamination for all values of θ.

Partial Local Delamination

The local delamination growing from an angle ply matrix crack modeled in fig.11b has a uniform delamination front across the laminate width. However, the local delaminations observed in the experiments have triangular shaped delamination areas that extend only partially into the laminate width from the free edge [1]. Therefore, an analysis was developed to account for the fact that the local delaminations in the $(0/\theta/-\theta)_s$ laminates did not extend across the entire laminate width, but instead were limited to the extent of the matrix crack in the $-\theta$ degree ply. The model was based on the assumption that the regions near the free edges containing the partial local delaminations act as a system of sublaminates in series, just as was assumed for the uniform local delamination, but this series system was assumed to be in parallel with the undamaged laminate in the interior of the laminate width (fig.11c).

Figure 15 shows three possible ways of visualizing the delamination growing from the matrix crack in the $-\theta$ degree ply. Fig. 15a shows a triangular shaped delamination that intersects the free edge at 90 degrees. Fig. 15b shows a triangular shaped delamination that intersects the matrix crack at 90 degrees. Finally, fig. 15c shows a triangular shaped delamination that intersects the free edge at an angle of 2θ. Eventually, if the local delamination in the $\theta/-\theta$ interface reaches a $+\theta$ degree matrix crack and arrests, the local delamination will appear to be an isosceles triangle with $+\theta$ and $-\theta$ angles intersecting the straight free edge. The relationship between the matrix crack length, d, and the delamination length along the free edge, a, is different for the three cases shown in fig. 15. These relationships are given in Table 4. Hence, the shape of the delamination front must be known in order to relate the delamination length on the free edge to the length of the matrix crack.

For a local delamination from a matrix crack, the compliance, S, where S = 1/E, for a laminate with a given local delamination area, A, in an interface whose total area is A^*, may be represented as (appendix 1)

$$\frac{S - S_{LAM}}{S^* - S_{LAM}} = \frac{A}{A^*} \tag{13}$$

where $S^* = 1/E^*_{LD}$, and $E^*_{LD} = (t_{LD}E_{LD})/t$ as defined in ref.2. Assuming a partial local delamination is present at a matrix crack on both free edges (fig.11c), and noting that a'=ka, where k is given in Table 4 for the three geometries shown in figures 15 a-c, then $A = maa' = mka^2$ and $A^* = 2mLka$. Substituting for A and A^* in eq(13) for any of these three geometries yields

$$S = \frac{1}{2}\left(\frac{1}{t_{LD}E_{LD}} - \frac{1}{tE_{LAM}}\right)\left(\frac{t}{L}\right)a + \frac{1}{E_{LAM}} \tag{14}$$

Recalling from ref.4 that, for a system in parallel,

$$G = -\frac{1}{2}V\varepsilon^2\frac{dE}{dA} \tag{15}$$

and noting that for the partial local delaminations shown in fig.11c $A = mka^2$, where k is given in Table 4 for the three geometries shown in figures 15 a-c, then $dA = 2mkada$. Substituting V = wLt and dA into eq(15) yields

$$G = -\frac{1}{2}\frac{wt\varepsilon^2}{2mk}\left(\frac{L}{a}\right)\frac{dE}{da} \tag{16}$$

The modulus of a laminate containing a delaminated region near the free edges loaded in parallel with an undamaged region in the interior of the laminate width is given by [4] as

$$E = (E^* - E_{LAM})\frac{A'}{(A')^*} + E_{LAM} \tag{17}$$

For the partial delamination case shown in fig. 11c, A' = 2mLa' and $(A')^* = mwL$. Substituting these expressions in eq(17), and noting that a'=ka, where k is given in Table 4 for the three geometries in fig. 15a-c, yields

$$E = (E^* - E_{LAM})\frac{2k}{w}a + E_{LAM} \qquad (18)$$

Unlike E^* calculated for edge delamination in eq(9), E^* in eq(18) is a function of the local delamination length along the free edge, a. Differentiating eq(18) with respect to a, and substituting into eq(16) yields

$$G = \frac{\varepsilon^2 t}{2m}\left(\frac{L}{a}\right)\left[E_{LAM} - E^* - a\frac{dE^*}{da}\right] \qquad (19)$$

Substituting $E^* = 1/S$, where S is given by eq(14), into eq(19) and differentiating yields

$$G = \frac{\varepsilon^2 t}{2m}\left(\frac{L}{a}\right)\left[E_{LAM} - \frac{1}{(Ba + C)} + \frac{Ba}{(Ba + C)^2}\right] \qquad (20)$$

where

$$B = \frac{1}{2}\left(\frac{1}{t_{LD}E_{LD}} - \frac{1}{tE_{LAM}}\right)\left(\frac{t}{L}\right) \qquad (21)$$

and

$$C = \frac{1}{E_{LAM}} \qquad (22)$$

Although the relationship between the matrix crack length, d, and the delamination length along the free edge, a, is different for the three cases shown in fig.15, eq.(20) is independent of k, and hence, G(a/L) is independent of the local delamination geometry assumed. However, as noted previously for eq(2), G in eq(20) will depend on the assumptions made when determining E_{LD} in eq(21). Therefore, B in eq(21), and hence G in eq(20), will depend on whether eqs. 5,6, or 7 are used to calculate E_{LD}. For the remainder of this paper, it will be assumed that the sublaminates that constitute the locally delaminated region experience both bending-extension and shear-extension coupling. Hence, eq(7) will be used to calculate E_{LD}.

Eq.(20) may be rearranged to yield

$$G = \frac{\varepsilon^2 t}{2m}\left(\frac{D}{C\left[D\left(\frac{a}{L}\right)+C\right]} + \frac{D}{\left[D\left(\frac{a}{L}\right)+C\right]^2}\right) \qquad (23)$$

where D = BL. When a/L = 0, then eq.(20) becomes

$$G = \frac{\varepsilon^2 t}{2m}\left(\frac{2D}{C^2}\right) \tag{24}$$

Substituting for D and C, normalizing by $\varepsilon^2 t$, and noting that $t_{LD}=4h$ and t=6h, eq(24) becomes

$$\frac{G}{\varepsilon^2 t} = \frac{3E_{LAM}^2}{2}\left(\frac{1}{4E_{LD}} - \frac{1}{6E_{LAM}}\right) \tag{25}$$

which is identical to eq(12) for the uniform local delamination.

Figs.16-19 compare normalized G values calculated using eq(23) for partial local delamination, as a function of delamination length along the free edge normalized by the laminate length, a/L, to normalized G values calculated from eq(12) for uniform local delamination and from eq(11) for edge delamination modeled in the θ/-θ interfaces of $(0/\theta/-\theta)_S$ laminates, where θ = 15, 20, 25, and 30 degrees, respectively. The uniform local delamination and edge delamination solutions are independent of delamination length, but for the partial local delamination solution, G decreases with increasing delamination length along the free edge. Both local delamination solutions yield greater normalized G values than the edge delamination solution for all delamination lengths.

Fig.20 shows G normalized by $\varepsilon^2 t$, as a function of a/L up to a/L=0.1, calculated using eq(20) for partial local delaminations in the θ/-θ interfaces of $(0/\theta/-\theta)_S$ laminates, where θ = 15, 20, 25, and 30 degrees. Normalized G values were only plotted for a/L values up to 0.1 because the magnitudes for small matrix crack lengths, and hence small delamination lengths, were of primary interest for comparing to experimental data. In each case, G decreases slightly with delamination length, unlike the solutions for uniform local delamination which were independent of delamination length. If the partial delamination geometry can be anticipated and linked to the matrix crack length as shown in fig.15a-c, then both the laminate toughness as a function of fatigue cycles and a critical matrix crack length would be needed to predict the onset of a partial local delamination in fatigue. However, as shown in fig.20, if the critical matrix crack length is sufficiently small, and hence, the corresponding delamination length along the free edge is small, the difference between the uniform and partial delamination solutions will be insignificant. In this case, G may be calculated from eq(2) to

compare to experimental data, even though the local delamination is not uniform across the laminate width.

Thermal/Moisture Contribution to G

The strain energy release rate for local delamination will be influenced by the presence of residual thermal and moisture stresses in the laminate. A uniform local delamination G solution that includes the effect of the mechanical load, the residual thermal stresses that exist in the laminate after it cools down from the curing temperature, and the hygroscopic stresses that exist in the laminate due to the presence of absorbed moisture, was recently developed [6]. Figs.21-24 show the contribution of mechanical load (M), temperature (T), and hygroscopic (H) moisture weight gain to G for a uniform local delamination in the $\theta/-\theta$ interfaces of $(0/\theta/-\theta)_s$ laminates (where θ = 15, 20, 25, and 30 degrees, respectively) subjected to a mechanical load of 3000 lb/in. and a ΔT of -156°C (-280°F). As shown in figs.21-24, when the contribution of the residual thermal stress is included, G^{M+T} will increase above the G^M value obtained from equation (2) for an applied mechanical load alone. However, when the presence of absorbed moisture is included, as may occur from exposure to the ambient air (appendix 3), the thermal stresses will relax and reduce the strain energy release rate, G^{M+T+H}, with increasing ΔH. Similar behavior was observed for edge delamination [7]. However, the magnitude of the thermal and moisture effects is much more significant for edge delamination. The laminates tested in this study had a moisture weight gain, ΔH, between 0.2 and 0.3 % (appendix 3). For the $(0/\theta/-\theta)_s$ laminates shown in figs. 21-24, this corresponds to a 5.8-7.7% increase in G^{M+T+H} compared to the G^M solution for mechanical loading only. The difference in G^{M+T+H} and G^M is even less at higher mechanical load levels (Table 5).

CORRELATION OF ANALYSIS AND EXPERIMENTS

Ideally, the closed form solutions for local delaminations from matrix cracks should be verified and calibrated by comparing them to detailed finite element solutions that sum the G components for the three fracture modes to obtain a total G. Such comparisons have been made for edge delamination [3-5]. However, to date only the case of uniform local delamination from 90 degree matrix cracks has been verified [8]. Part of the difficulty is that the modelling for

local delamination requires a full 3D analysis, with the matrix crack geometry modeled accurately. The solutions for non-90 degree matrix cracks that have been attempted to date [9,10], have assumed that the angle ply matrix cracks may be represented as straight cracks through the laminate thickness that are normal to the $\theta_2/-\theta_2$ interface. However, as seen in micrographs of the edges for the $(0_2/\theta_2/-\theta_2)_s$ laminates [1], these angle ply matrix cracks are curved, intersecting the ply interface at oblique angles. This difference in actual versus assumed matrix crack geometry through the laminate thickness may have a significant effect on the G components calculated from a finite element analysis for local delamination.

Although the fatigue behavior of the $(0_2/\theta_2/-\theta_2)_s$ laminates cannot currently be predicted, it may be possible to correlate the fatigue delamination onset behavior between laminates with different values of θ. The data from each layup may be used to generate delamination onset criteria by generating plots of maximum cyclic G versus the number of cycles to delamination onset for the composite material. A similar characterization has been used previously for edge delamination data [5,11].

Laminate and sublaminate moduli for the $(0_2/\theta_2/-\theta_2)_s$ AS4/3501-6 graphite epoxy laminates were calculated using the properties in table 3 in laminated plate theory. The moduli of the locally delaminated regions, E_{LD}, were calculated using eq(7) to incorporate the influence of bending-extension and shear-extension coupling. These moduli were then used in eq(2), along with the maximum cyclic loads in the fatigue tests, to calculate strain energy release rates for uniform local delaminations corresponding to the measured number of cycles to delamination onset for each layup. In addition, the matrix crack length, d, corresponding to the number of cycles for local delamination onset was measured from the X-ray radiographs where local delamination was first observed for each specimen. Examination of the partial local delaminations in these radiographs indicated that the geometry shown in fig. 15c was reasonable for the layups tested. Therefore, measured matrix crack lengths, d, were used in the expression in Table 4 corresponding to fig.15c to determine critical delamination lengths along the free edge, a, at local delamination onset for each layup. Table 6 shows the range of delamination lengths along the free edge, a, normalized by the gage length, L, measured just after local delamination onset in fatigue. These critical delamination lengths were used, along with the maximum cyclic loads in the fatigue tests, to calculate strain energy release rates from eq(20) for partial local delaminations

corresponding for the measured number of cycles to delamination onset for each layup. Hence, plots of G_{max} versus the number of cycles to delamination onset, N, were generated for each layup assuming either uniform, or partial, local delamination onset from a $-\theta$ degree matrix ply crack.

Figure 25 shows the G_{max} vs. N plot for both the uniform and partial local delamination models. The maximum cyclic G levels for the uniform and partial local delamination models are very similar because the experimentally determined critical delamination lengths were small (Table 6, fig.20). In addition, for any particular maximum cyclic load, the maximum cyclic G levels for all values of θ also agree fairly well, indicating that the assumptions of shear-extension and bending-extension coupling reflected in eq(7) was accurate (fig.12). Finally, the number of cycles to delamination onset at each cyclic G level appear to be greater for the 15 and 20 degree cases than for the 25 and 30 degree cases. These differences in the number of cycles to delamination onset may be due to a difference in either the mixed-mode ratio, or the extent of matrix cracking prior to delamination onset, for the individual cases. Neither of these effects are incorporated in the current analyses.

Figure 26 shows the G_{max} vs. N plot for the uniform local delamination models with mechanical loading only, G^M, and with mechanical, thermal, and hygroscopic loading combined, G^{M+T+H}. For any particular maximum cyclic load, the maximum cyclic G^{M+T+H} is only slightly greater than the the maximum cyclic G^M because of the relatively small contribution of the residual thermal and moisture stresses to G (Table 5).

The G_{max} vs. N plots in figures 25 and 26 provide some insight into the accuracy of the G solutions derived in this paper. However, as noted earlier, a detailed analysis of the G components and a mixed-mode fatigue failure criterion for this material may be needed to predict the fatigue behavior of these $(0_2/\theta_2/-\theta_2)_s$ laminates.

CONCLUSIONS

Constant amplitude tension-tension fatigue tests were conducted on AS4/3501-6 graphite epoxy $(0_2/\theta_2/-\theta_2)_s$ laminates, where θ was 15, 20, 25,and 30 degrees. Fatigue tests were conducted at a frequency of 5 Hz and an R-ratio of 0.1. Dye penetrant enhanced X-ray radiography was used to document the onset of matrix cracking in the central $-\theta$ degree plies, and the subsequent onset of local delaminations in the $\theta/-\theta$ interface at the intersection of the matrix cracks and the free edge, as a function of the number of fatigue cycles. Unlike the quasi-static tests [1], the sequence of damage was evident in the series of radiographs taken during the cyclic loading, with the matrix cracking always preceding the onset of local delamination.

Two strain energy release rate solutions for local delamination from matrix cracks were derived: one for a local delamination growing from an angle ply matrix crack with a uniform delamination front across the laminate width, and one for a local delamination growing from an angle ply matrix crack with a triangular shaped delamination area that extended only partially into the laminate width from the free edge. Plots of G_{max} vs. N were generated to assess the accuracy of these G solutions. The influence of residual thermal and moisture stresses on G were also quantified. However, a detailed analysis of the G components and a mixed-mode fatigue failure criterion for this material may be needed to predict the fatigue behavior of these laminates.

REFERENCES

1. O'Brien, T.K., and Hooper, S.J., "Local Delamination in Laminates with Angle Ply Matrix Cracks: Part I, Tension Tests and Stress Analysis," NASA TM 104055, 1991, to be presented at the 4th ASTM Symposium on Composite Materials: Fatigue and Fracture, Indianapolis, Indiana, May, 1991.

2. O'Brien,T.K., "Analysis of Local Delaminations and Their Influence on Composite Laminate Behavior," Delamination and Debonding of Materials, ASTM STP 876, 1985, pp.282-297.

3. O'Brien,T.K., Johnston,N.J., Raju,I.S., and Morris,D.H., "Comparisons of Various Configurations of the Edge Delamination Test for Interlaminar Fracture Toughness," Toughened Composites, ASTM STP 937, 1987, pp.199-221.

4. O'Brien,T.K., "Characterization of Delamination Onset and Growth in a Composite Laminate," Damage in Composite Materials, ASTM STP 775, 1982, pp.140-167.

5. O'Brien,T.K., "Mixed-mode Strain Energy Release Rate Effects on Edge Delamination of Composites," Effects of Defects in Composite Materials, ASTM STP 836, 1984, pp.125-142.

6. O'Brien, T.K., "Residual Thermal and Moisture Influences on the Strain Energy Release Rate Analysis of Local Delaminations from Matrix Cracks," NASA TM 104077, 1991, Submitted to the ASTM Journal of Composites Technology and Research.

7. O'Brien, T.K., Raju, I.S., and Garber, D.P., "Residual Thermal and Moisture Influences on the Strain Energy Release Rate Analysis of Edge Delamination," J. Composites Technology and Research, Vol.8, No.2, Summer, 1986.

8. Salpekar,S.A., and O'Brien,T.K., "Combined Effect of Matrix Cracking and Free Edge on Delamination," Composite Materials: Fatigue and Fracture, 3rd Volume, ASTM STP 1110, 1991.

9. Fish,J.C., and O'Brien,T.K., "Three-Dimensional Finite Element Analysis of Delamination from Matrix Cracks in Glass-Epoxy Laminates," Composite Materials: Testing and Design, 10th Volume, ASTM STP 1120, 1992.

10. Salpekar,S.A., and O'Brien,T.K., "Analysis of Matrix cracking and Local Delamination in $(0/\theta/-\theta)_S$ Graphite Epoxy Laminates under Tension Load," ICCM VIII, Honolulu, Proceedings, July, 1991.

11. Adams, D.F., Zimmerman,R.S., and Odom,E.M., "Frequency and Load Ratio Effects on Critical Strain Energy Release Rate G_C Thresholds of Graphite /Epoxy Composites, " Toughened Composites, ASTM STP 937, 1987, pp.242-259.

APPENDIX 1 - UNIFORM LOCAL DELAMINATION FROM AN ANGLE PLY MATRIX CRACK

For a local delamination from a matrix crack, the laminate compliance, S, where S = 1/E, for a laminate with a given local delamination area, A, in an interface whose total area is A^*, may be represented as

$$\frac{S - S_{LAM}}{S^* - S_{LAM}} = \frac{A}{A^*} \qquad (A1)$$

where $S^* = 1/E^*_{LD}$, and $E^*_{LD} = (t_{LD}E_{LD})/t$ as defined in ref.2. Fig. 11a shows the uniform local delamination that extends across the entire laminate width and grows normal to a 90 degree matrix ply crack in the load direction. For the uniform delamination in fig. 11a, A = mwa, and A^* = mwL, where m=2 for an interior matrix crack and m=1 for a matrix crack in a surface ply. Substituting these expressions into eq(A1) yields

$$S = \left(\frac{1}{t_{LD}E_{LD}} - \frac{1}{tE_{LAM}}\right)\left(\frac{t}{L}\right)a + \frac{1}{E_{LAM}} \qquad (A2)$$

which is identical to eq(7) in ref.2 for local delamination from a 90 degree matrix ply crack.

Fig. 11b shows the uniform local delamination that extends across the entire laminate width and grows from a -θ degree matrix ply crack normal to the load direction. For the uniform delamination in fig. 11b, A= (mw/sinθ) (a sinθ) = mwa, and A^* = mwL. Substituting these expressions into eq(A1) also yields eq(A2).

For the 90 degree matrix crack induced local delamination in fig 11a, dA = mwda. Similarly, for the -θ degree matrix crack induced local delamination in fig. 11b, dA = (mw/sinθ) d(a sinθ) = mwda. In ref.2, G is defined as

$$G = \frac{1}{2} V\sigma^2 \frac{dS}{dA} \qquad (A3)$$

Substituting for V = wLt and dA = mwda and differentiating eq (A2) with respect to "a" yields

$$G = \frac{P^2}{2mw^2}\left(\frac{1}{t_{LD}E_{LD}} - \frac{1}{t_{LAM}E_{LAM}}\right) \qquad \text{(A4)}$$

for uniform local delaminations from either a 90 degree or a -θ degree matrix crack.

APPENDIX 2 - ANALYSIS OF MODULI FOR ASYMMETRIC SUBLAMINATES

In laminated plate theory, the load and moment resultants are related to the midplane strains and curvatures as

$$\begin{Bmatrix} N \\ M \end{Bmatrix} = \begin{bmatrix} A & B \\ B & D \end{bmatrix} \begin{Bmatrix} \varepsilon \\ \kappa \end{Bmatrix} \qquad \text{(A5)}$$

where A, D, and B represent the extensional, bending, and bending-extension coupling matrices, respectively. By prescribing an applied mechanical strain, $\varepsilon_x = \varepsilon_0$, setting the applied N_y, N_{xy}, and M_y equal to 0, and setting κ_x and κ_{xy} equal to 0, eq(A5) becomes

$$\begin{Bmatrix} N_x \\ 0 \\ 0 \\ \hline M_x \\ 0 \\ M_{xy} \end{Bmatrix} = \begin{bmatrix} A & B \\ B & D \end{bmatrix} \begin{Bmatrix} \varepsilon_0 \\ \varepsilon_y \\ \gamma_{xy} \\ \hline 0 \\ \kappa_y \\ 0 \end{Bmatrix} \qquad \text{(A6)}$$

The three equations whose left hand side are zero may be written as

$$\begin{aligned} -A_{12}\varepsilon_0 &= A_{22}\varepsilon_y + A_{26}\gamma_{xy} + B_{22}\kappa_y \\ -A_{16}\varepsilon_0 &= A_{26}\varepsilon_y + A_{66}\gamma_{xy} + B_{26}\kappa_y \\ -B_{12}\varepsilon_0 &= B_{22}\varepsilon_y + B_{26}\gamma_{xy} + D_{22}\kappa_y \end{aligned} \qquad \text{(A7)}$$

where $A_{ij}=A_{ji}$. This set of three non-homogeneous equations may be solved for ε_y, γ_{xy}, and κ_{xy} using Cramer's rule. Hence,

$$\varepsilon_y = \frac{D_1}{D}\varepsilon_0, \quad \gamma_{xy} = \frac{D_2}{D}\varepsilon_0, \quad \kappa_y = \frac{D_3}{D}\varepsilon_0 \qquad \text{(A8)}$$

where

$$D_1 = \begin{vmatrix} -A_{12} & A_{26} & B_{22} \\ -A_{16} & A_{66} & B_{26} \\ -B_{12} & B_{26} & D_{22} \end{vmatrix}$$

$$D_2 = \begin{vmatrix} A_{22} & -A_{12} & B_{22} \\ A_{26} & -A_{16} & B_{26} \\ B_{22} & -B_{12} & D_{22} \end{vmatrix}$$

$$D_3 = \begin{vmatrix} A_{22} & A_{26} & -A_{12} \\ A_{26} & A_{66} & -A_{16} \\ B_{22} & B_{26} & -B_{12} \end{vmatrix}$$

and

$$D = \begin{vmatrix} A_{22} & A_{26} & B_{22} \\ A_{26} & A_{66} & B_{26} \\ B_{22} & B_{26} & D_{22} \end{vmatrix}$$

These expressions for ε_y, γ_{xy}, and κ_{xy} may be substituted into the first equation of eqs(A6) to yield

$$N_x = \left[A_{11} + \left(\frac{D_1}{D}\right)A_{12} + \left(\frac{D_2}{D}\right)A_{16} + \left(\frac{D_3}{D}\right)B_{12}\right]\varepsilon_0 \qquad \text{(A9)}$$

Hence, N_x may be obtained explicitly as a function of the terms in the A, B, and D matrices and the prescribed axial strain, ε_0. Then noting that

$$E_{LD} = \frac{2N_x}{(N\text{-}n)h\varepsilon_0} \qquad \text{(A10)}$$

yields

$$E_{LD} = \frac{2}{(N\text{-}n)h}\left[A_{11} + \left(\frac{D_1}{D}\right)A_{12} + \left(\frac{D_2}{D}\right)A_{16} + \left(\frac{D_3}{D}\right)B_{12}\right] \qquad \text{(A11)}$$

By prescribing the loading outlined above, but setting $\gamma_{xy} = 0$ instead of prescribing that $N_{xy} = 0$, i.e., by prescribing an applied

mechanical strain, $\varepsilon_x = \varepsilon_0$, setting the applied N_y and M_y equal to 0, and setting γ_{xy}, κ_x, and κ_{xy} equal to 0, eq(A5) becomes

$$\begin{Bmatrix} N_x \\ 0 \\ N_{xy} \\ \hline M_x \\ 0 \\ M_{xy} \end{Bmatrix} = \begin{bmatrix} A & B \\ B & D \end{bmatrix} \begin{Bmatrix} \varepsilon_0 \\ \varepsilon_y \\ 0 \\ \hline 0 \\ \kappa_y \\ 0 \end{Bmatrix} \tag{A12}$$

The two equations whose left hand side are zero are

$$0 = A_{12}\varepsilon_0 + A_{22}\varepsilon_y + B_{22}\kappa_y \tag{A13}$$

$$0 = B_{12}\varepsilon_0 + B_{22}\varepsilon_y + D_{22}\kappa_y \tag{A14}$$

where $A_{ij}=A_{ji}$ and $B_{ij}=B_{ji}$. Multiplying eq(A13) by $-D_{22}$, multiplying eq(A14) by B_{22}, and then adding the two equations yields

$$\varepsilon_y = \left(\frac{B_{12}B_{22} - A_{12}D_{22}}{A_{22}D_{22} - B_{22}B_{22}}\right)\varepsilon_0 \tag{A15}$$

Furthermore, multiplying eq(A13) by $-B_{22}$, multiplying eq(A14) by A_{22}, and adding the two equations yields

$$\kappa_y = \left(\frac{A_{12}B_{22} - A_{22}B_{12}}{A_{22}D_{22} - B_{22}B_{22}}\right)\varepsilon_0 \tag{A16}$$

Finally, substituting eqs(A15) and (A16) into the first equation of eq(A12) yields

$$N_x = \left[A_{11} - \left(\frac{A_{12}D_{22} - B_{12}B_{22}}{A_{22}D_{22} - B_{22}B_{22}}\right)A_{12} + \left(\frac{A_{12}B_{22} - A_{22}B_{12}}{A_{22}D_{22} - B_{22}B_{22}}\right)B_{12}\right]\varepsilon_0 \tag{A17}$$

Hence, N_x may be obtained explicitly as a function of the terms in the A, B, and D matrices and the prescribed axial strain, ε_0. Then recalling eq(A10)

$$E_{LD} = \frac{2N_x}{(N-n)h\varepsilon_0}$$

and substituting the expression for N_x from eq(A17) yields

$$E_{LD} = \frac{2}{(N-n)h}\left[A_{11} - \left(\frac{A_{12}D_{22} - B_{12}B_{22}}{A_{22}D_{22} - B_{22}B_{22}}\right)A_{12} + \left(\frac{A_{12}B_{22} - A_{22}B_{12}}{A_{22}D_{22} - B_{22}B_{22}}\right)B_{12}\right] \quad \text{(A18)}$$

APPENDIX 3 - MOISTURE CONTENT DETERMINATION

Just prior to testing the $(0_2/\theta_2/-\theta_2)_S$ laminates, two control coupons of each layup were weighed, dried, and then weighed again to determine ΔH for the laminates in the ambient environment. These dried control specimens were then weighed periodically to identify their moisture content by weight as a function of time.

Fig. 27 shows the percentage moisture content by weight, ΔH, as a function of the number of days from the time the specimens were dried. There was very little difference in the percentage moisture weight gain for the different layups. The percentage difference in the original weight measured just before drying and the weight measured immediately after the specimens were dried was approximately 0.2% for all the layups. This value is shown in fig.27 as the original ambient condition. Because all of the fatigue data were generated within a period of 30 days, the percentage moisture weight gain for all the laminates that were tested in fatigue was assumed to be between 0.2% and 0.3%.

ACKNOWLEDGEMENTS

The author would like to thank Kathy Long and Kim Benton for their support in conducting the fatigue testing, and Adrian Benson for his assistance with data reduction and plotting during the course of this study.

TABLE 1

X-ray Schedule for $(0_2/\theta_2/-\theta_2)_s$ Fatigue Tests

P_{max}, N (lbs)	X-ray taken every N cycles	Between N_1 cycles	and N_2 cycles
26,690 (6000)	1000	1	5000
22,240 (5000)	1000	1	5000
17,790 (4000)	1000 2000	1 10,000	10,000 20,000
15,570 (3500)	1000 2000 5000 10,000	1 10,000 20,000 50,000	10,000 20,000 50,000 110,000
13,340 (3000)	1 ,000 50,000	1 100,000	100,000 1,000,000

TABLE 2 - Average Number of Martrix Cracks at Local Delamination Onset in $(0_2/\theta_2/-\theta_2)_s$ AS4/3501-6 Graphite Epoxy Laminates

	θ, degrees			
P_{max} , N (lbs)	15	20	25	30
Static Test	1.35	1.57	2.67	5.25
17,790 (4000)	14.2	9.7	11.0	20.7
15,570 (3500)	12.0	10.3	13.7	23.3
13,340 (3000)	9.0	14.0	15.7	32.0

TABLE 3 - AS4/3501-6 Graphite Epoxy Lamina Properties

E_{11} = 135 GPa (19.5 x 10^6 Psi)

E_{22} = 11 GPa (1.6 x 10^6 Psi)

G_{12} = 5.8 GPa (0.847 x 10^6 Psi)

ν_{12} = 0.301

α_1 = -0.41 x10^{-6} /°C (-0.23 x10^{-6} /°F)

α_2 = 26.8 x10^{-6} /°C (14.9 x10^{-6} /°F)

β_1 = 0.00 /weight %

β_2 = 5.56 x10^{-3} /weight %

TABLE 4 - Partial Local Delamination Geometries

Configuration	d	a'	k
Fig. 26a	$\frac{a}{\sin\theta}$	a $\tan\theta$	$\tan\theta$
Fig. 26b	a $\cos\theta$	a $\cos\theta \sin\theta$	$\cos\theta \sin\theta$
Fig. 26c	$a\left(\cos\theta - \frac{\sin\theta}{\tan 3\theta}\right)$	$a \sin\theta \left(\cos\theta - \frac{\sin\theta}{\tan 3\theta}\right)$	$\sin\theta \left(\cos\theta - \frac{\sin\theta}{\tan 3\theta}\right)$

TABLE 5 - Percentage Difference between G^{M} and G^{M+T+H} for $\Delta H = 0.3\%$

	θ, degrees			
P_{max} , N (lbs)	15	20	25	30
13,340 (3000)	5.8%	7.5%	7.7%	7.0%
15,570 (3500)	5.0%	6.6%	6.8%	6.1%
17,790 (4000)	4.3%	5.8%	6.2%	5.8%
22,240 (5000)	3.7%	4.9%	5.1%	4.9%

TABLE 6 - Range of Critical Normalized Delamination Lengths at the Free Edge of $(0_2/\theta_2/-\theta_2)_s$ Graphite Epoxy Laminates Measured After Local Delamination Onset in Fatigue

θ, Degrees	a/L
15	.034-.106
20	.036-.090
25	.029-.063
30	.019-.062

Fig. 1a. RADIOGRAPH OF $(0_2/20_2/-20_2)_s$ LAMINATE AFTER MATRIX CRACKING ONSET IN FATIGUE

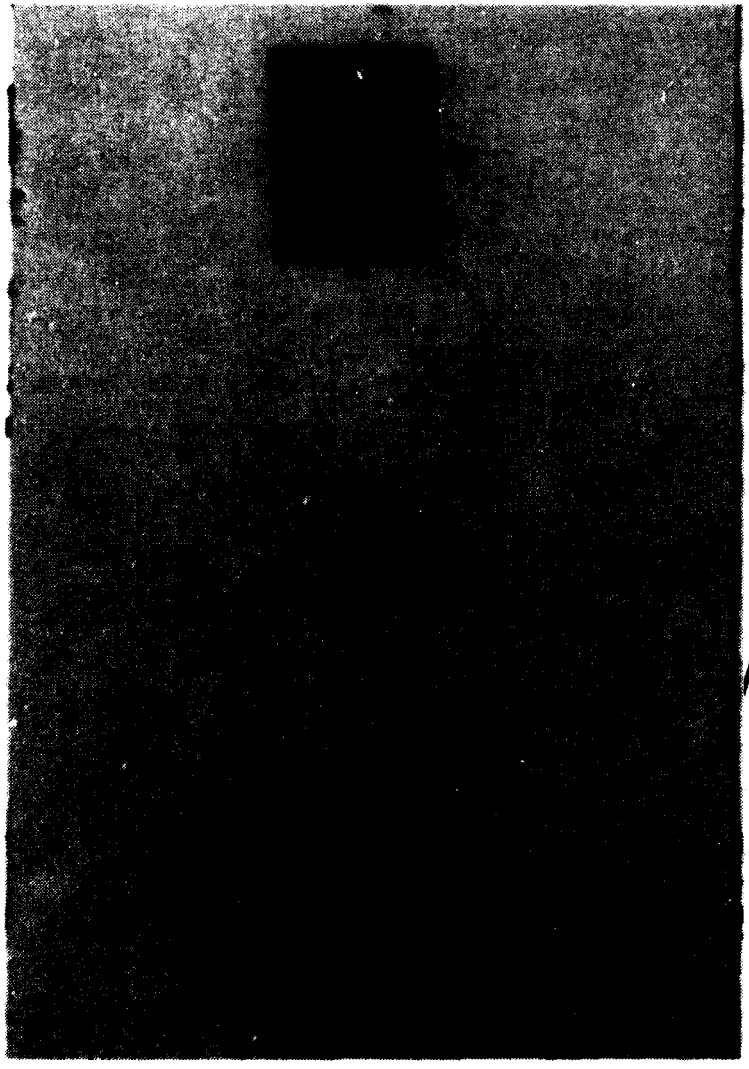

Fig. 1b. RADIOGRAPH OF $(0_2/20_2/-20_2)_s$ LAMINATE AFTER LOCAL DELAMINATION ONSET IN FATIGUE

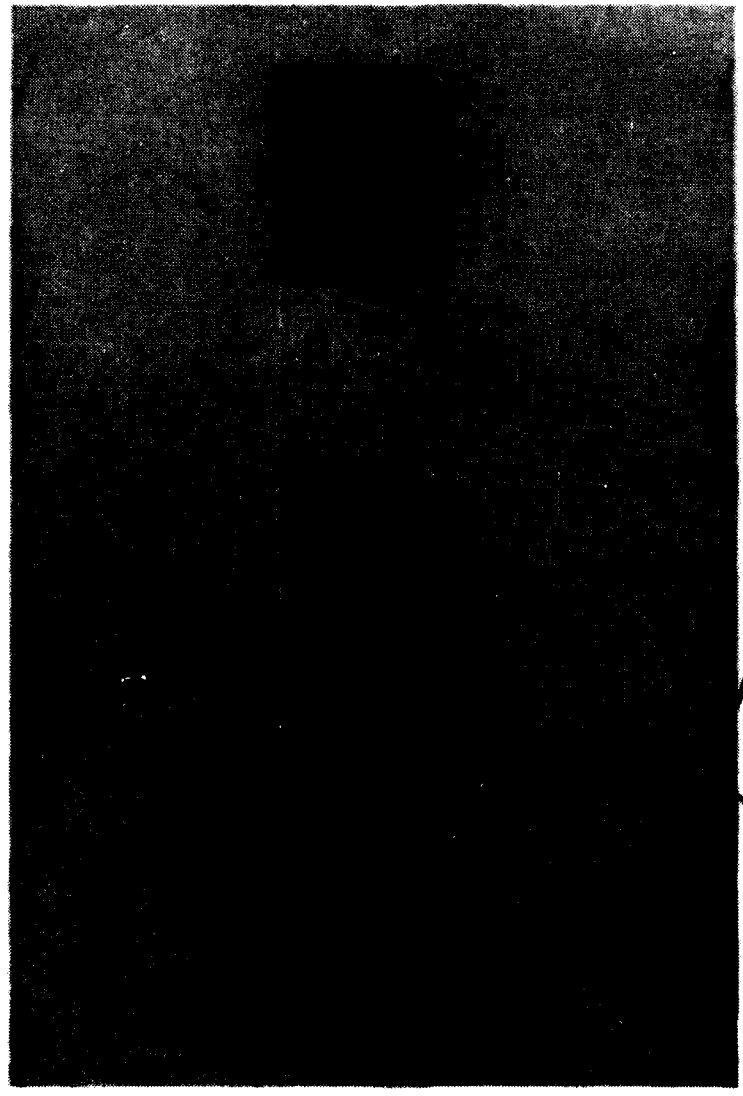

Fig. 2. PHOTOMICROGRAPHS OF EDGE OF $[0_2/20_2/-20_2]_s$ AS4/3501-6 GRAPHITE EPOXY FATIGUE SPECIMENS

P_{MAX} = 5000 lbs

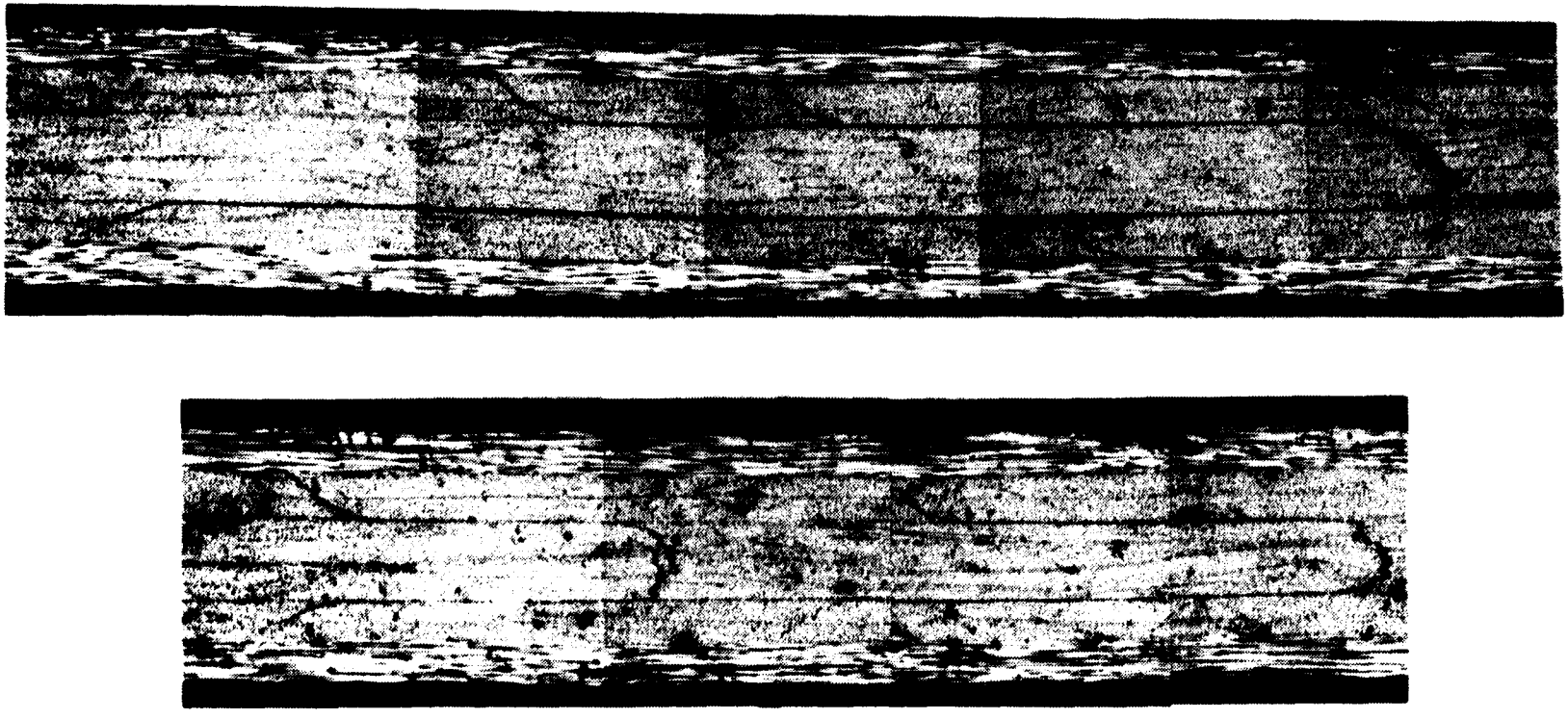

FIG.3 $[0_2/15_2/-15_2]_s$ FATIGUE

AS4/3501-6

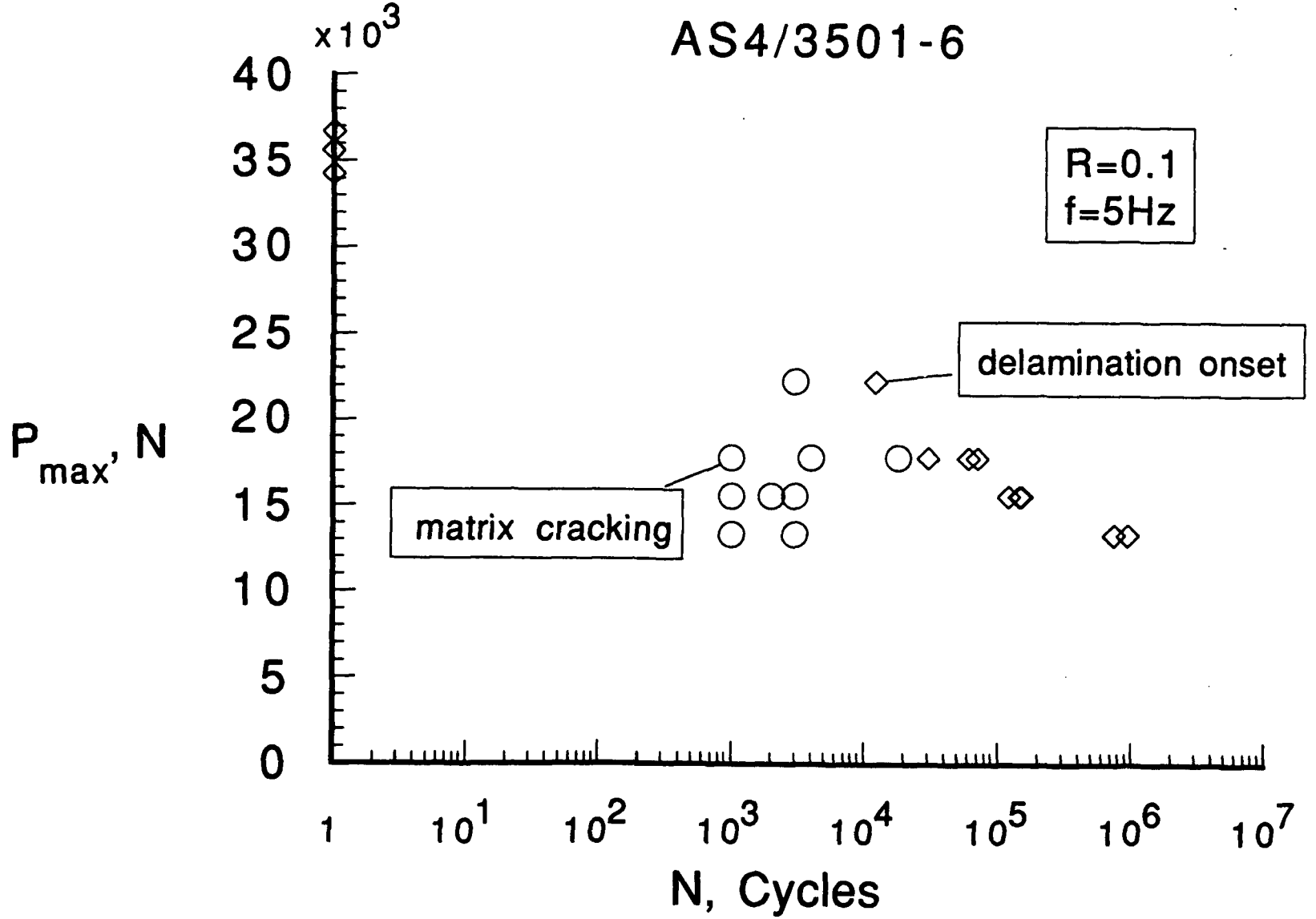

FIG.4 $[0_2/20_2/-20_2]_s$ FATIGUE

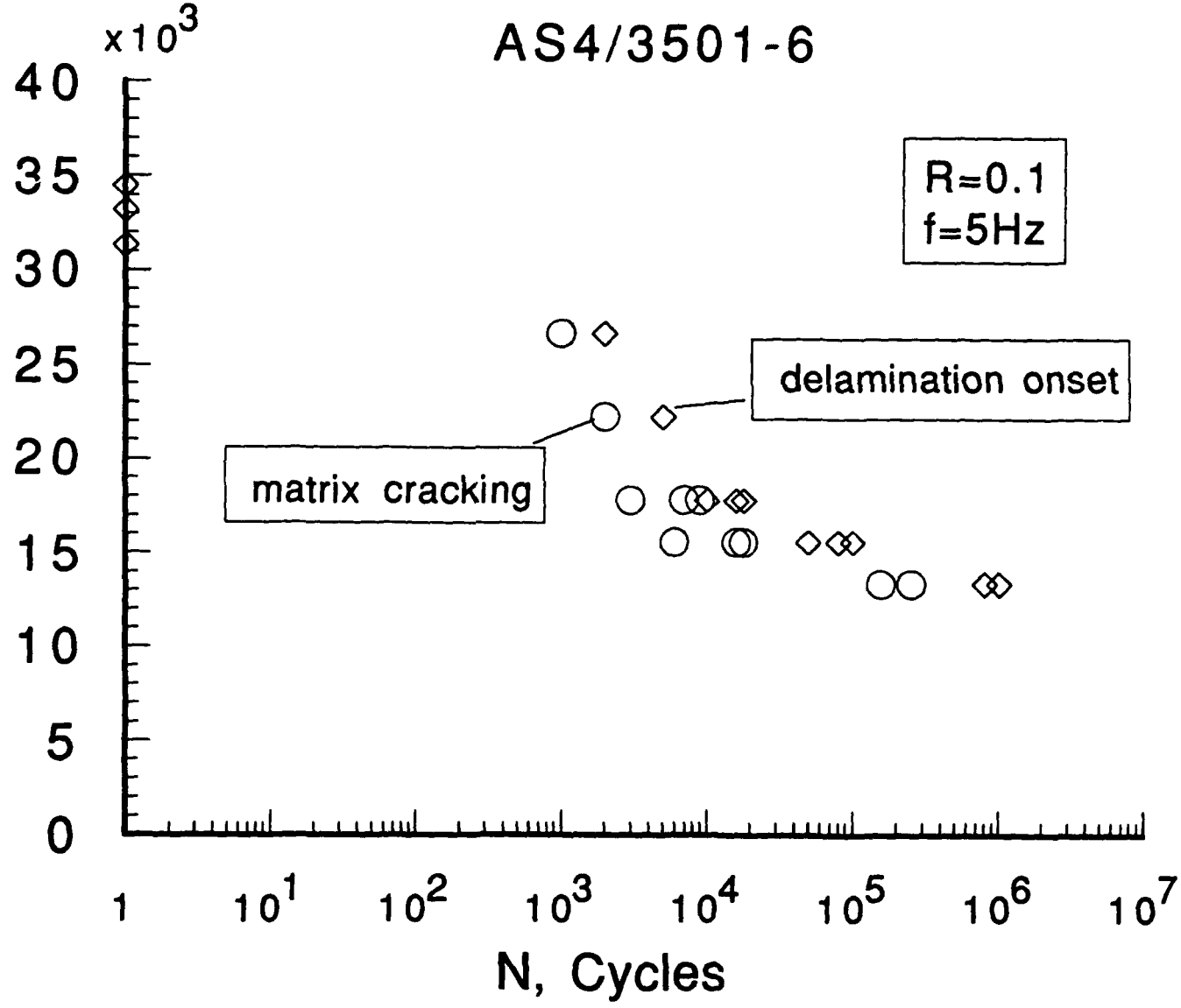

FIG.5 $[0_2/25_2/-25_2]_s$ FATIGUE
AS4/3501-6

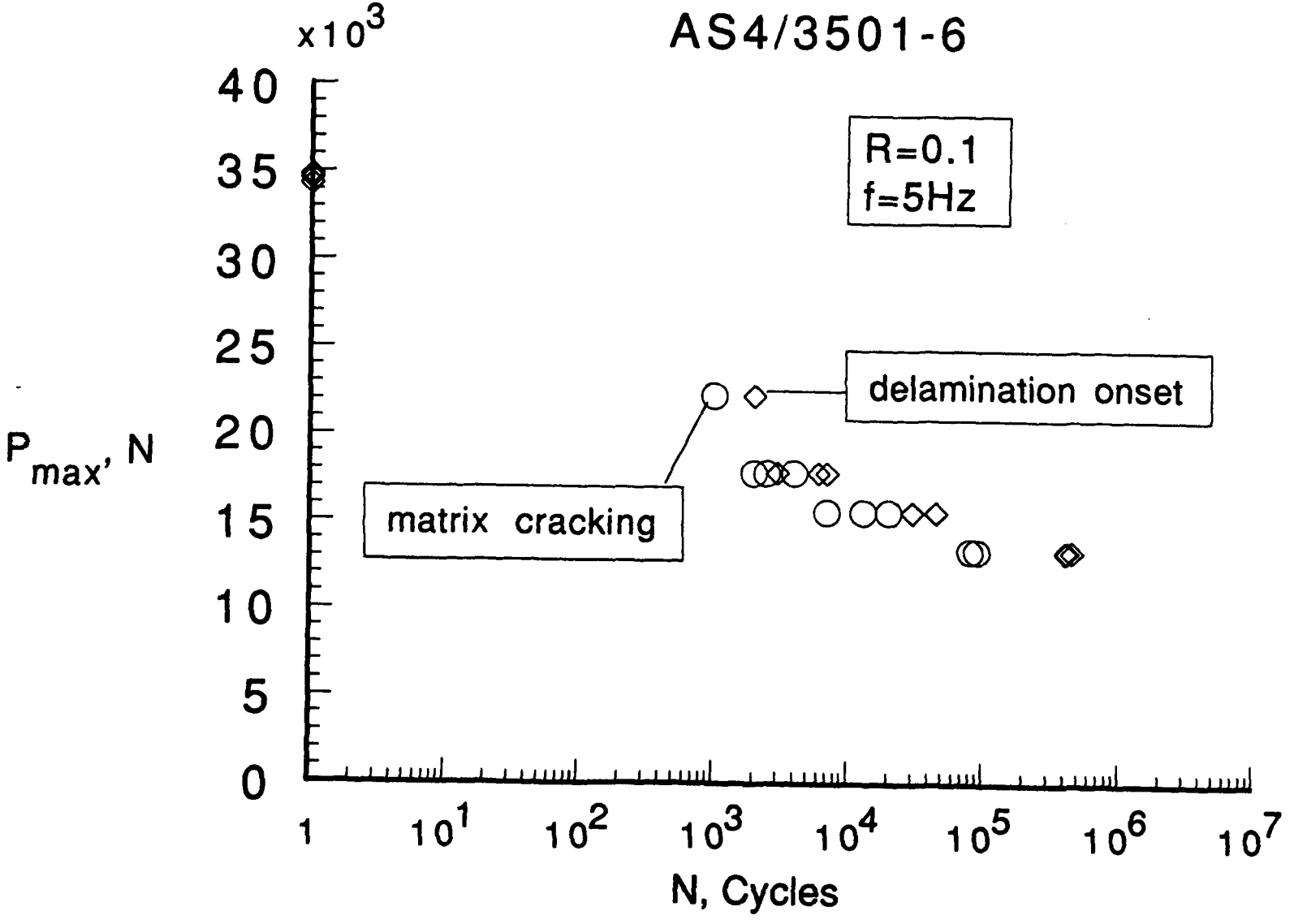

FIG.6 $[0_2/30_2/-30_2]_s$ FATIGUE

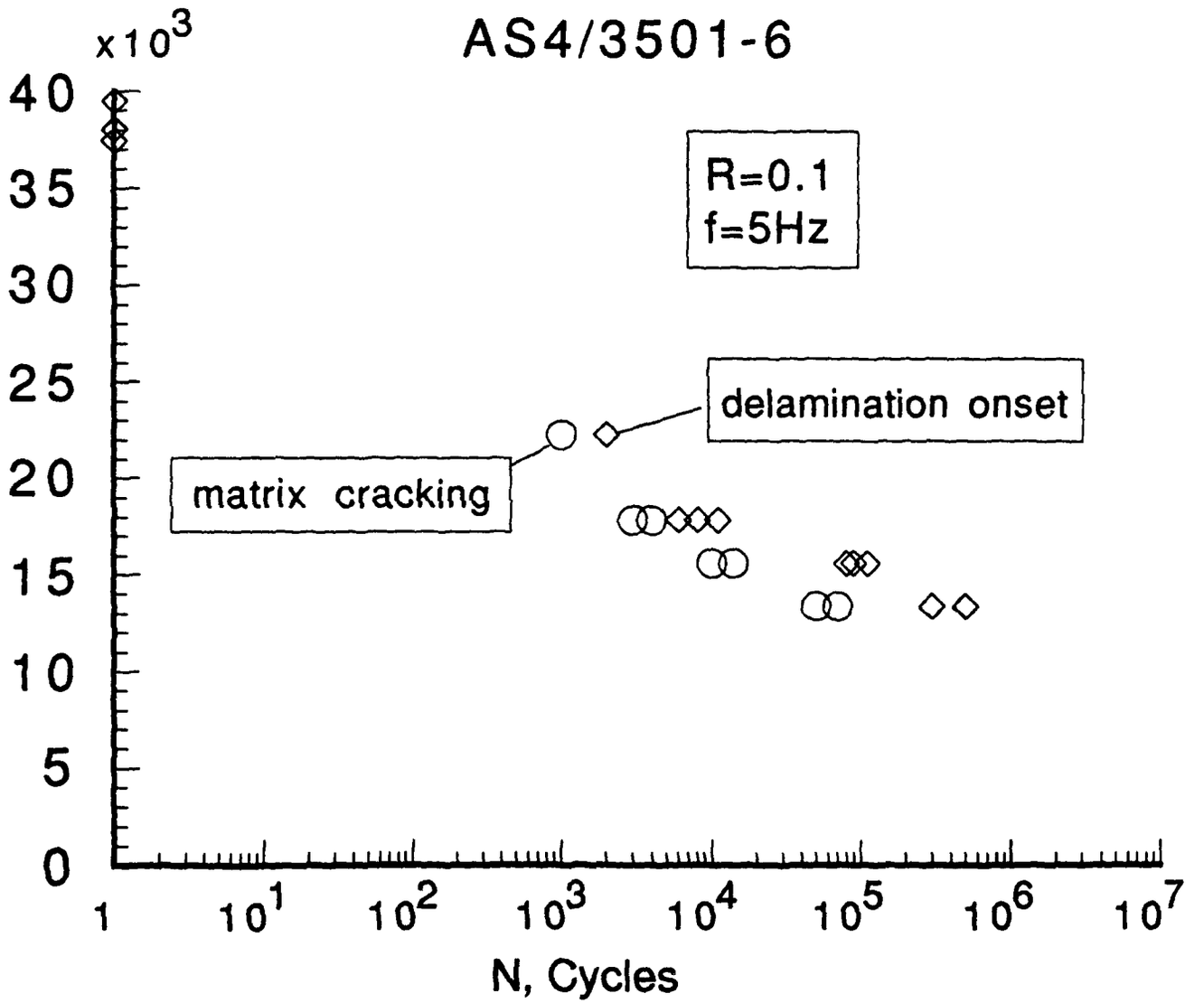

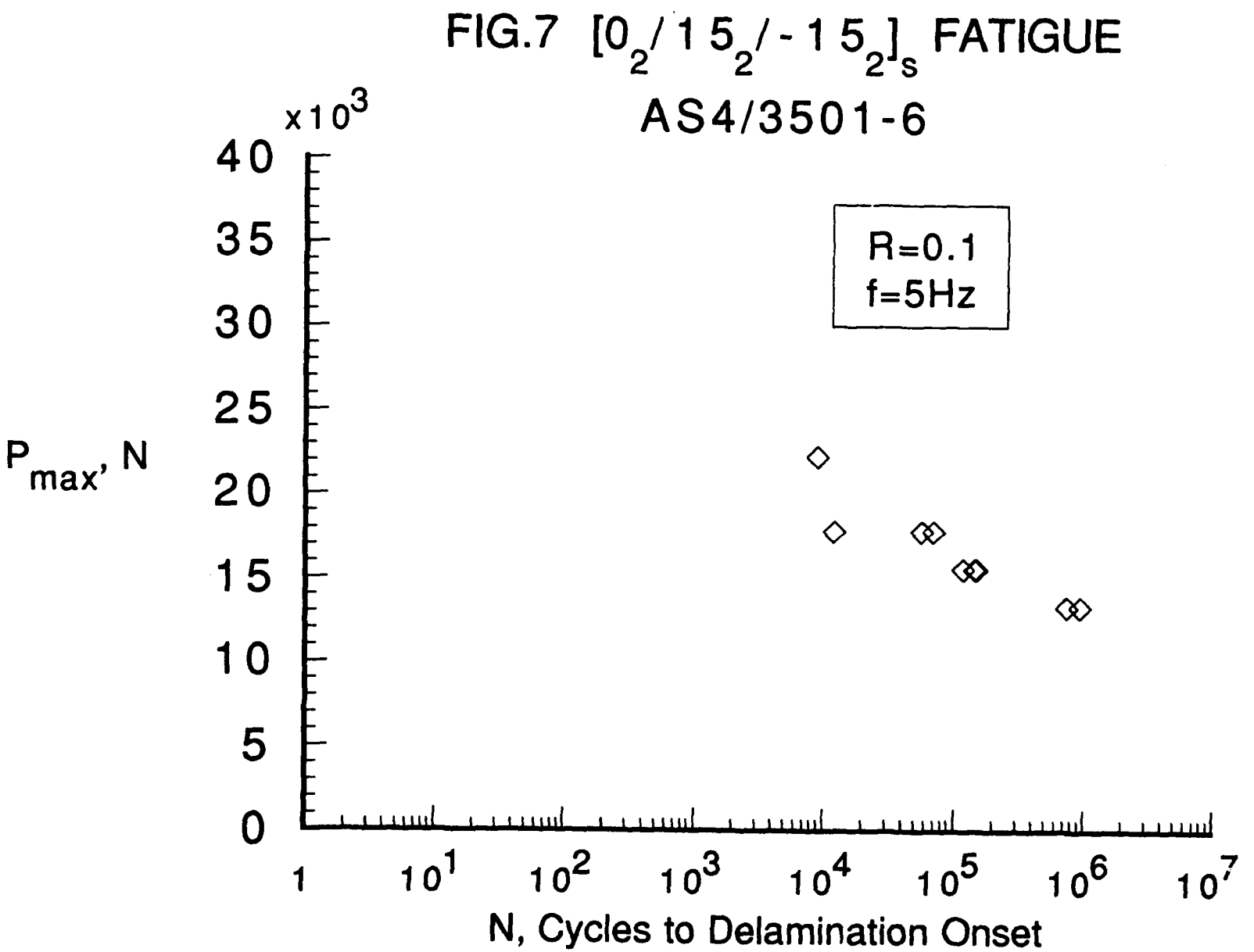
FIG.7 [0₂/15₂/-15₂]s FATIGUE
AS4/3501-6
x10³
40
35
30
25
20
15
10
5
0
Pmax, N
R=0.1
f=5Hz
1
10¹
10²
10³
10⁴
10⁵
10⁶
10⁷
N, Cycles to Delamination Onset

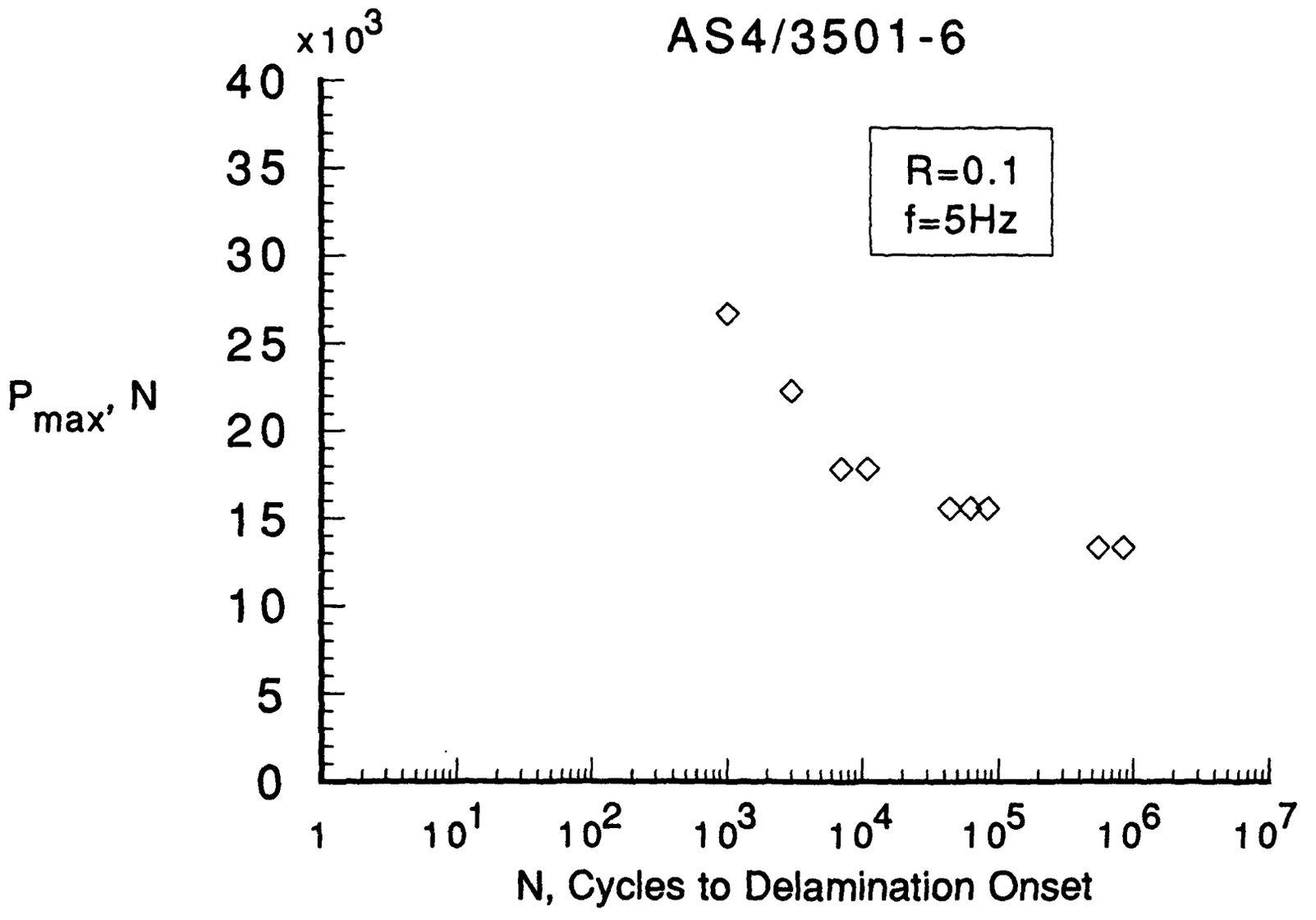
FIG.8 [0₂/20₂/-20₂]s FATIGUE
AS4/3501-6
x10³
40
35
30
25
20
15
10
5
0
P max, N
R=0.1
f=5Hz
1
10¹
10²
10³
10⁴
10⁵
10⁶
10⁷
N, Cycles to Delamination Onset

FIG.9 $[0_2/25_2/-25_2]_s$ FATIGUE
AS4/3501-6

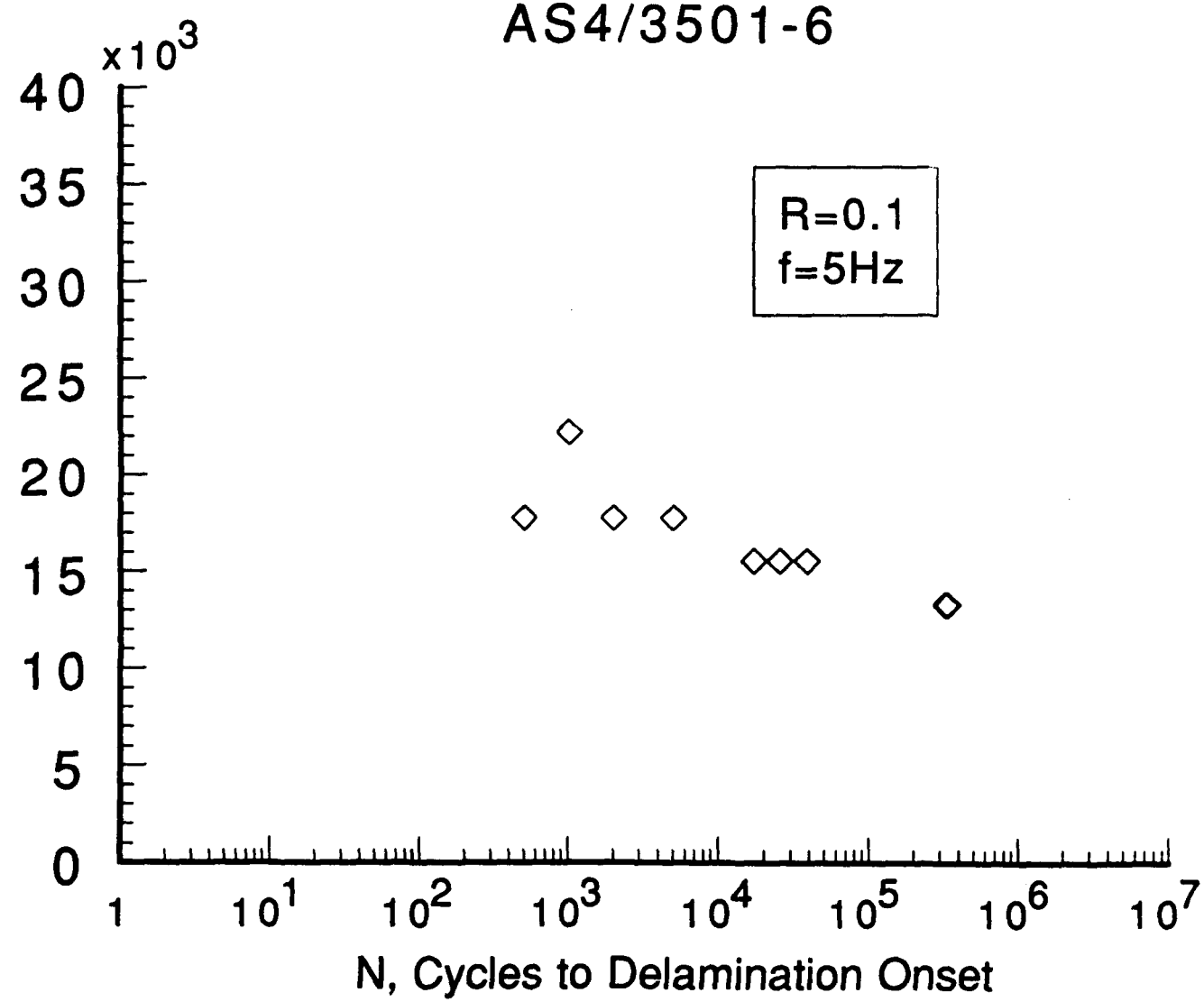

FIG.10 $[0_2/30_2/-30_2]_s$ FATIGUE
AS4/3501-6

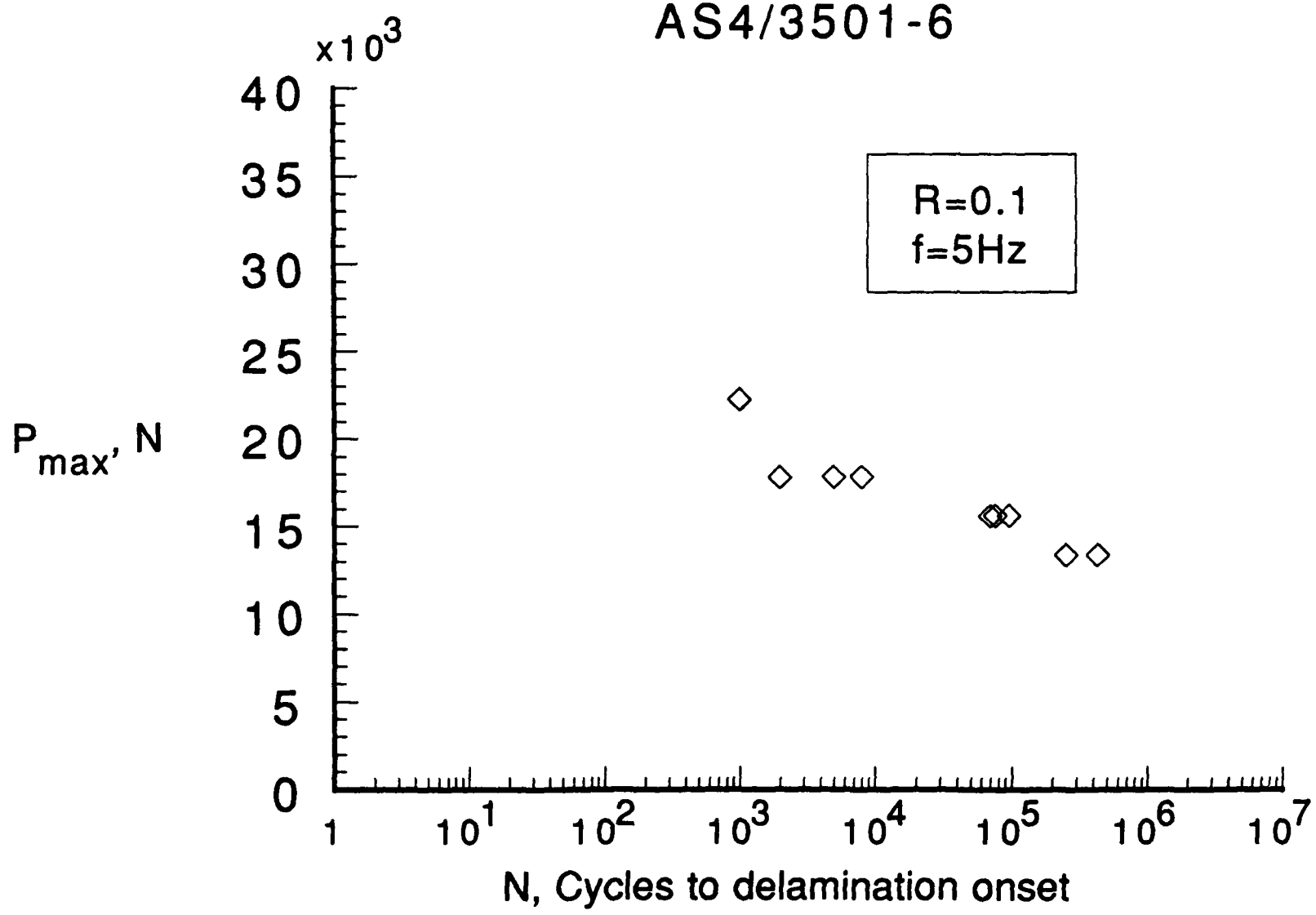

Fig. 11. LOCAL DELAMINATION MODELS

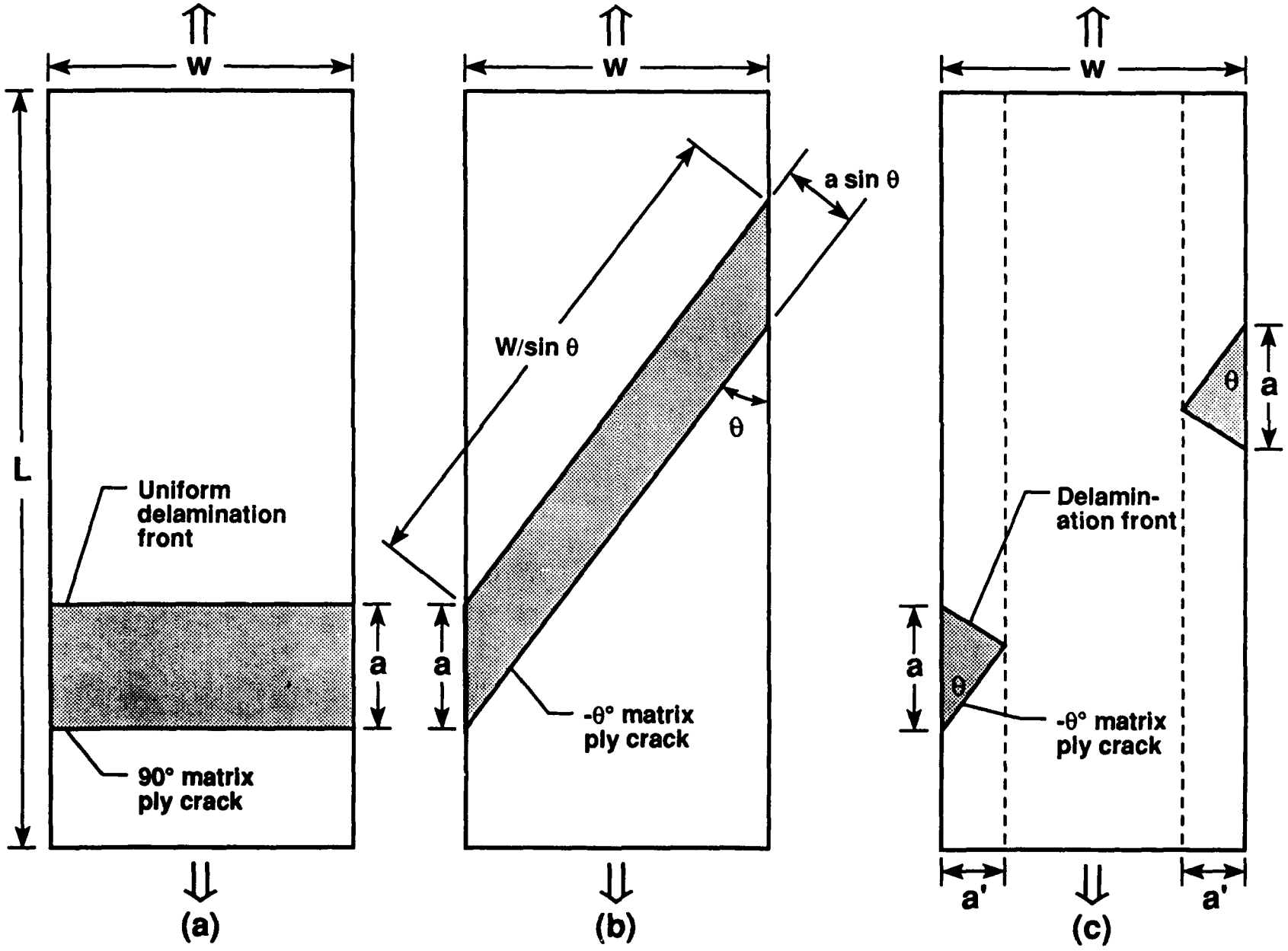

FIG.12 Normalized G for Uniform Local Delamination in θ/ -θ Interface of $(0/\theta/ -\theta)_s$ Laminates

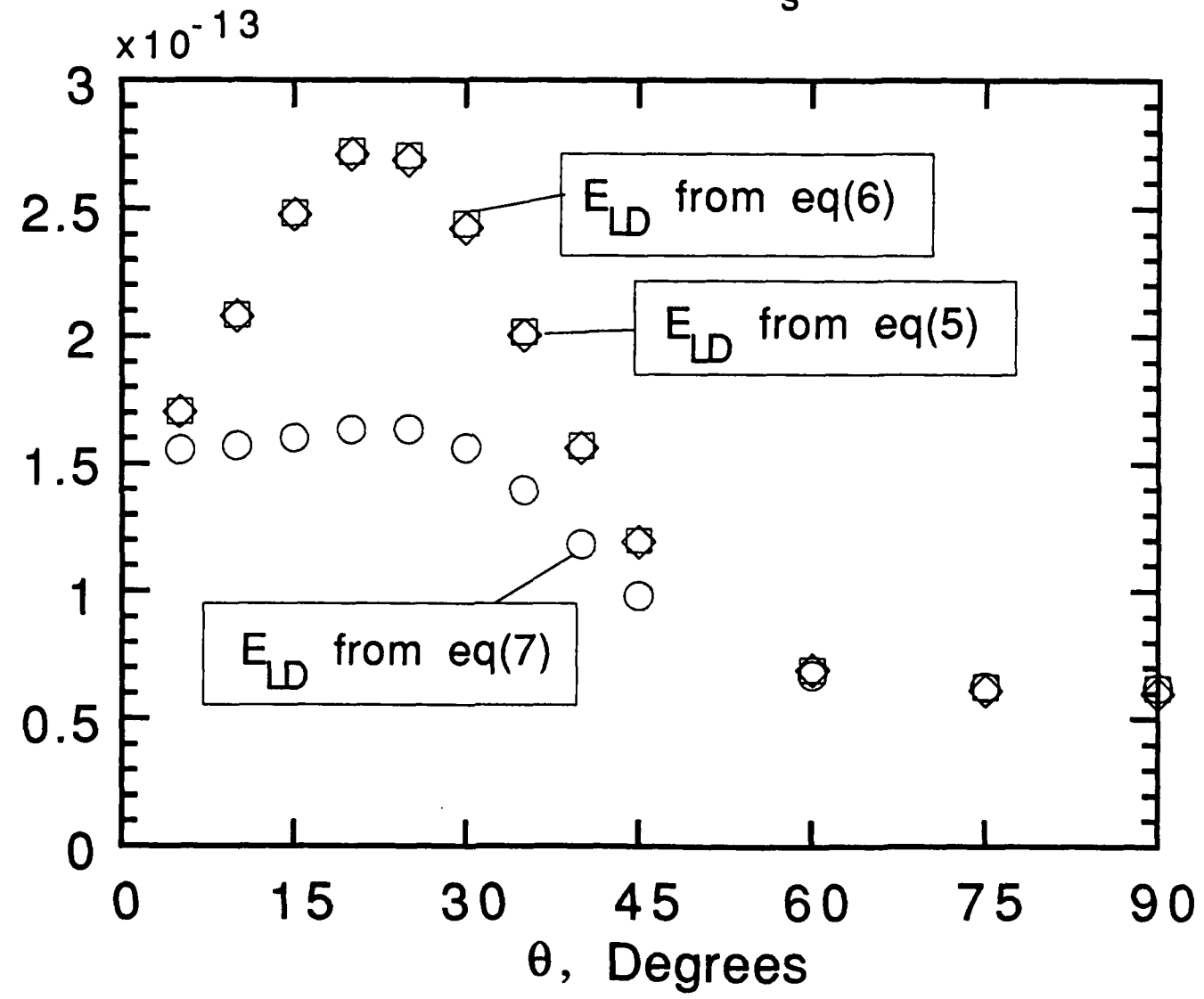

FIG.13 Normalized G for Edge Delamination in θ/ -θ Interface of $(0/\theta/-\theta)_s$ Laminates

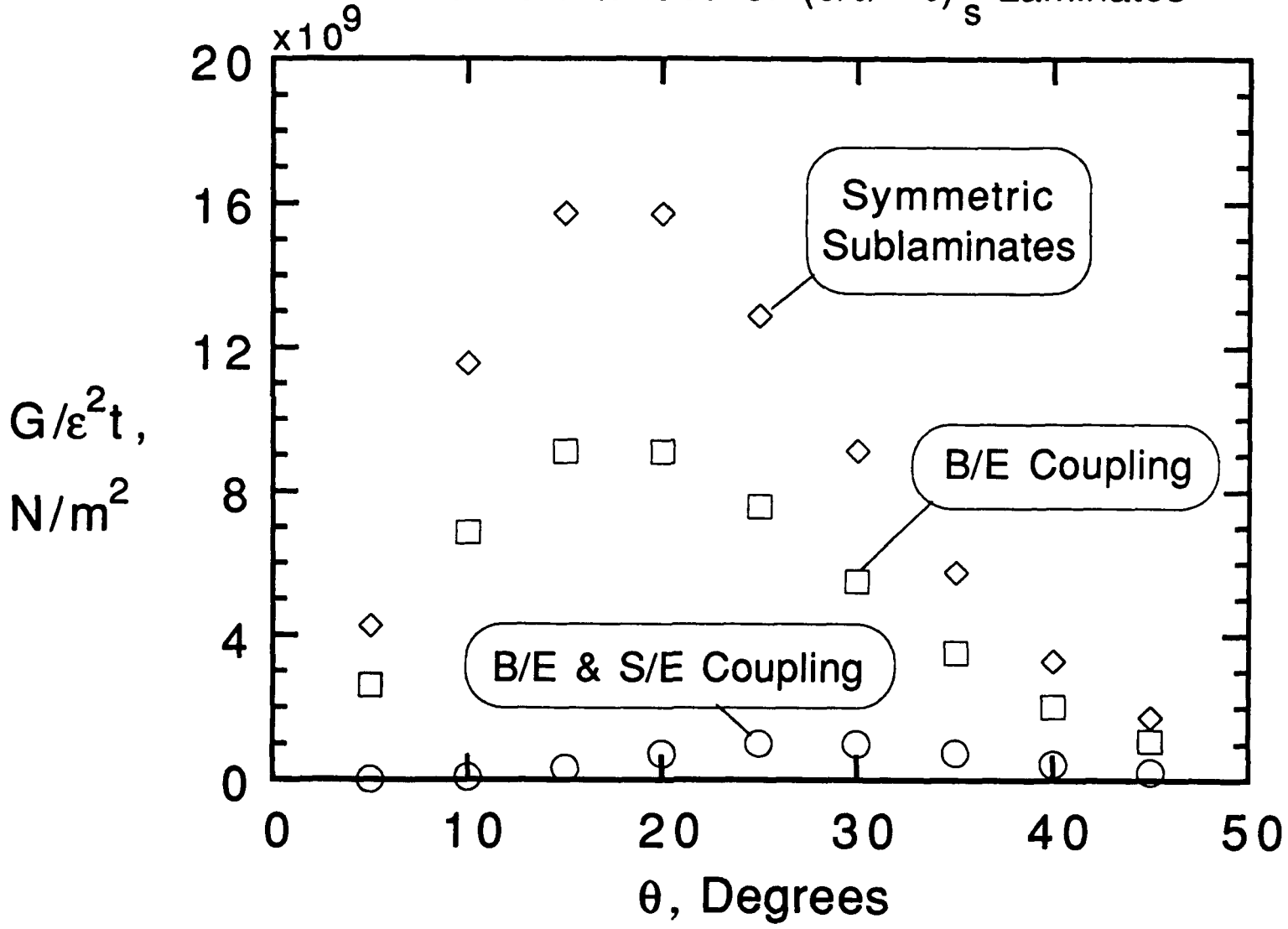

FIG.14 Normalized G for Delamination in θ/ -θ interfaces of $(0/\theta/-\theta)_s$ Laminates

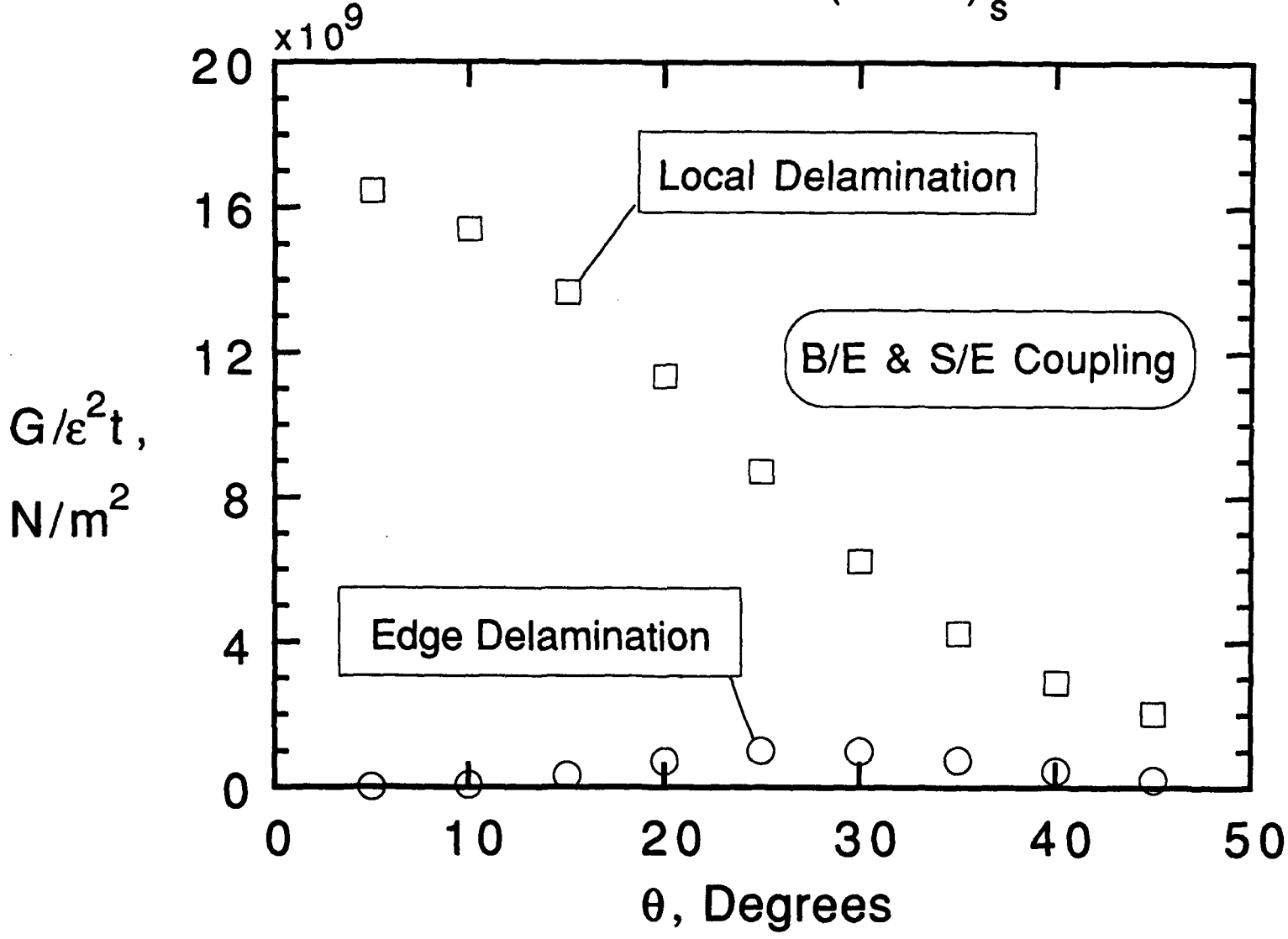

Fig. 15. PARTIAL LOCAL DELAMINATION GEOMETRIES

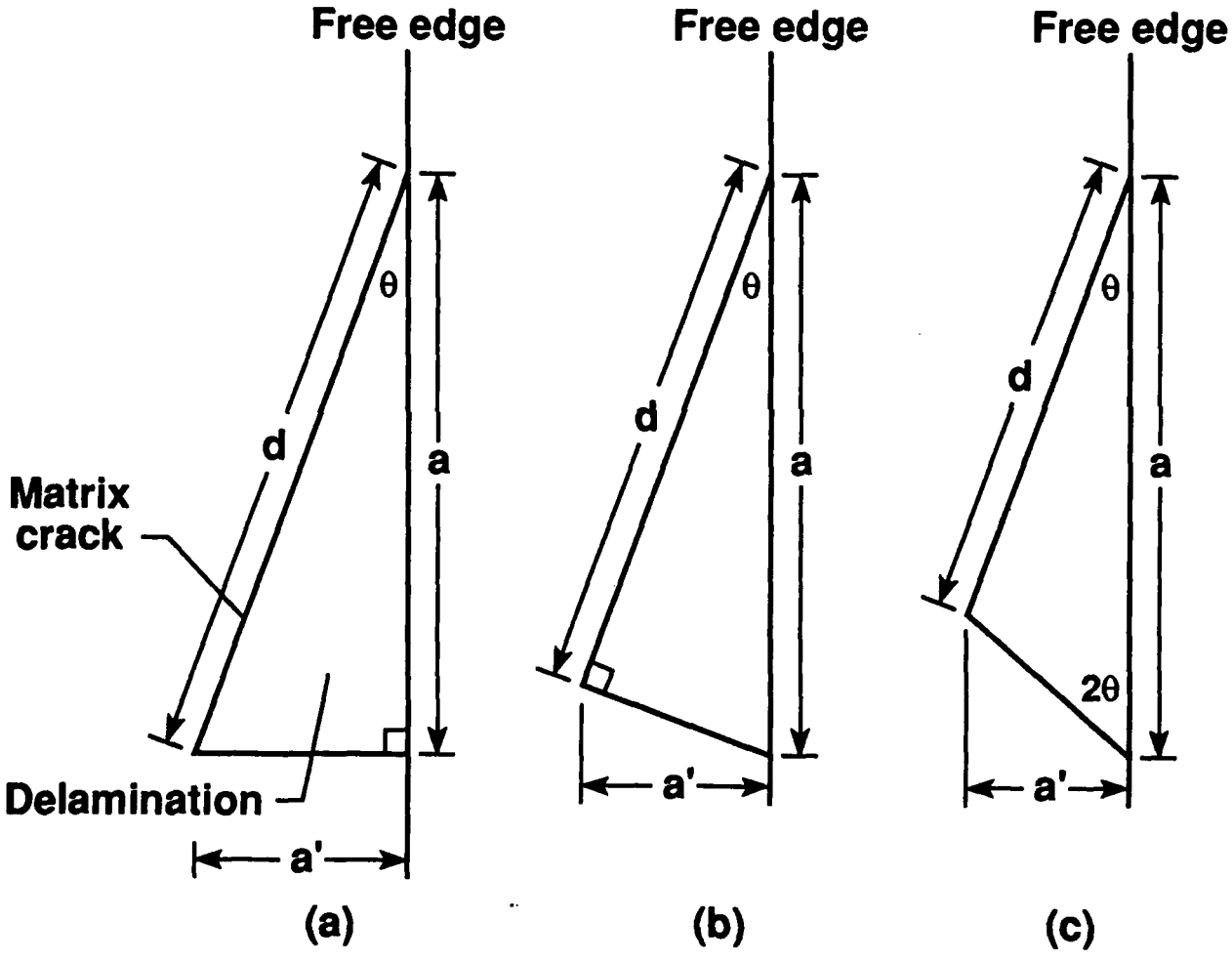

FIG.16 Normalized G for Delamination in 15/-15 Interface of $(0/15/-15)_s$ Laminate

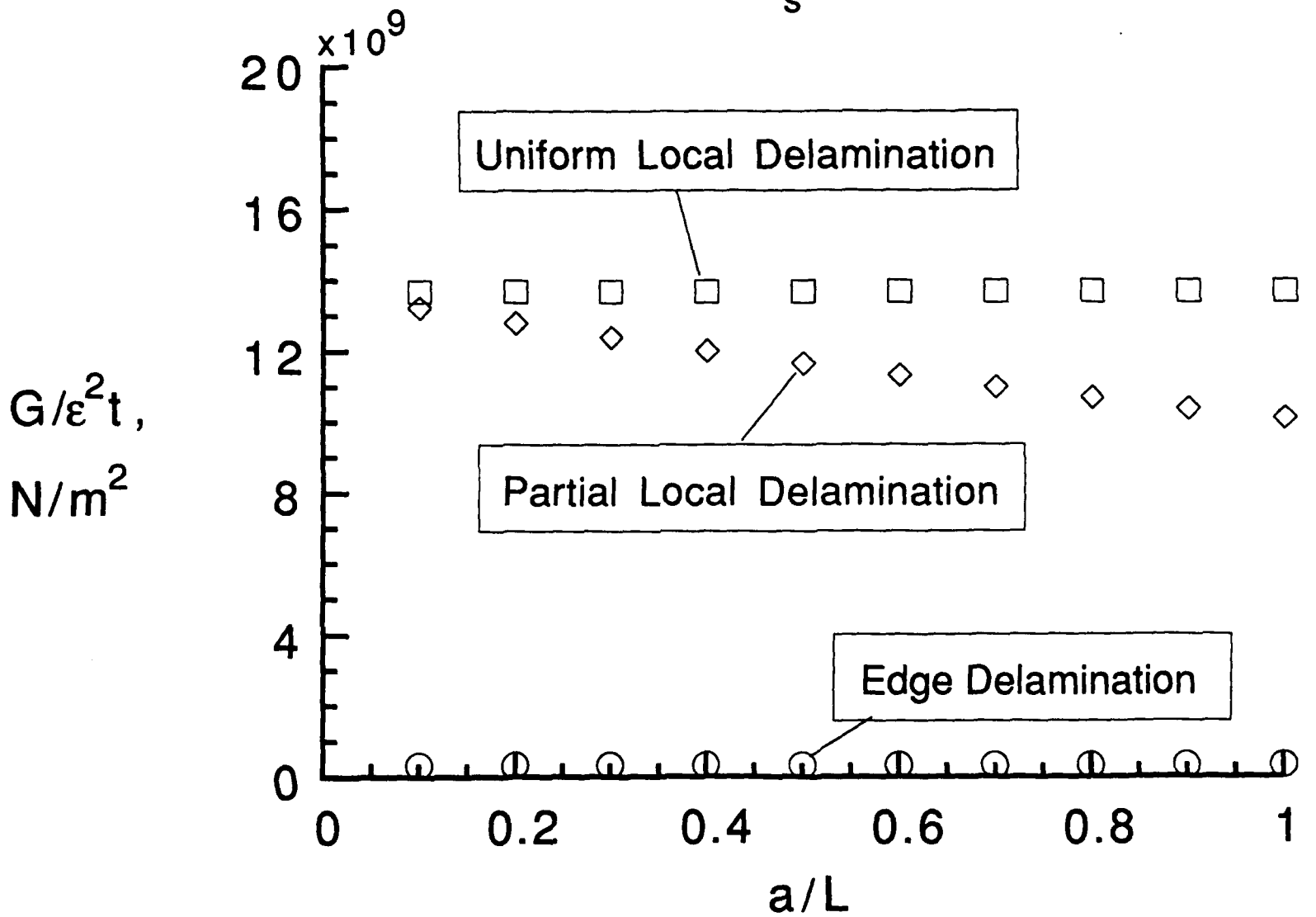

FIG.17 Normalized G for Delamination in 20/-20 Interface of $(0/20/-20)_s$ Laminate

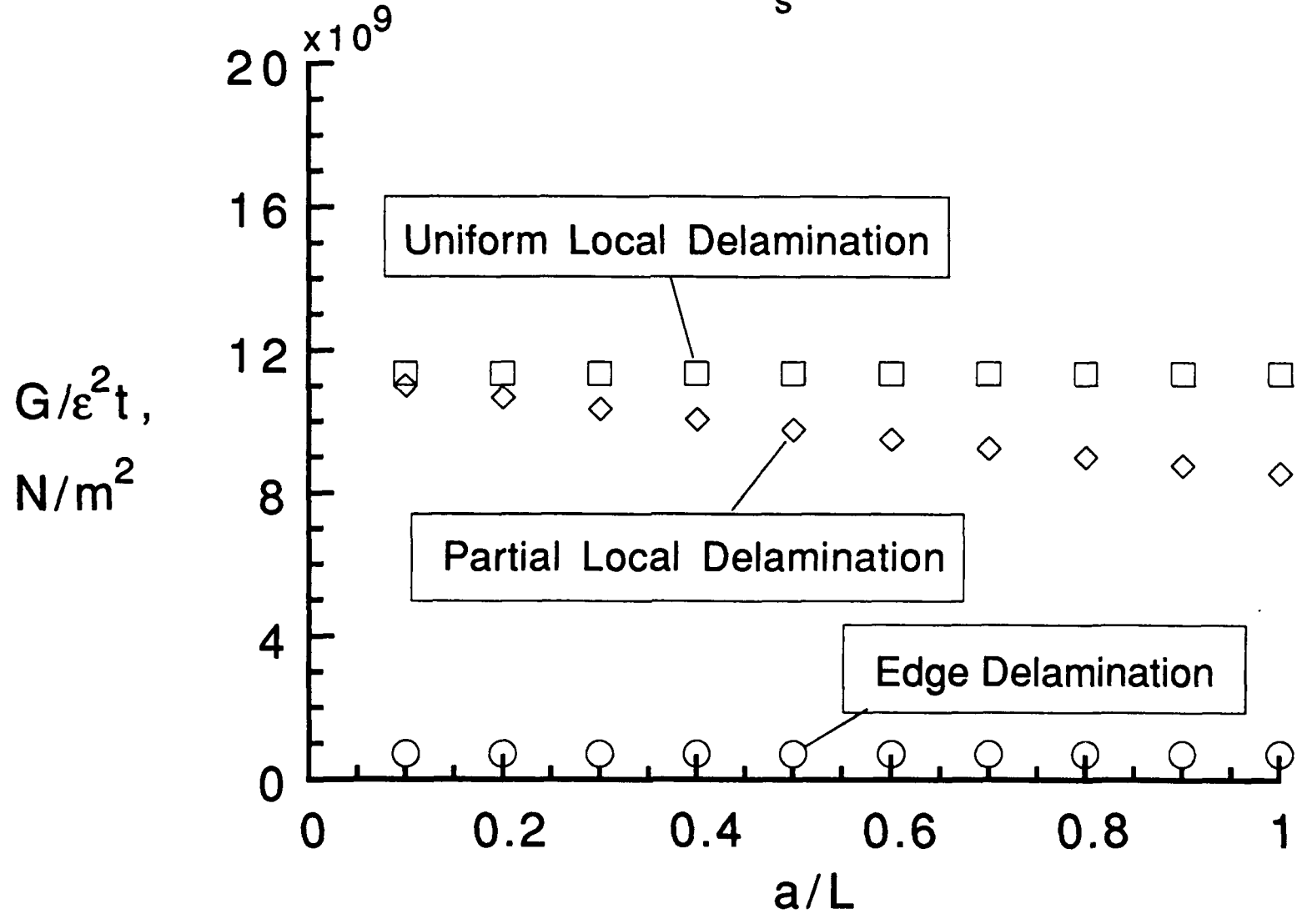

FIG.18 Normalized G for Delamination in 25/-25 Interface of $(0/25/-25)_s$ Laminate

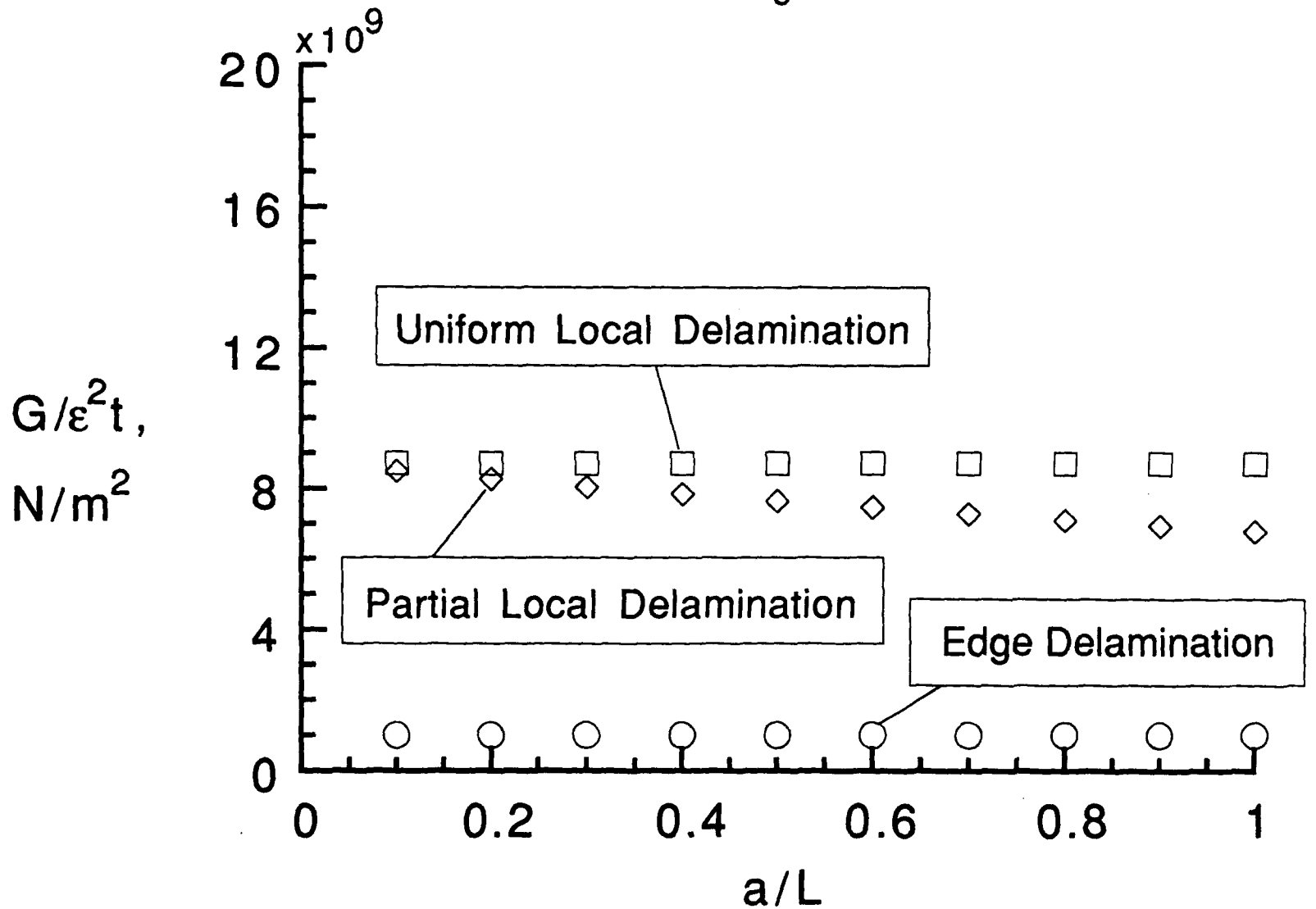

FIG.19 Normalized G for Delamination in 30/-30 Interface of $(0/30/-30)_s$ Laminate

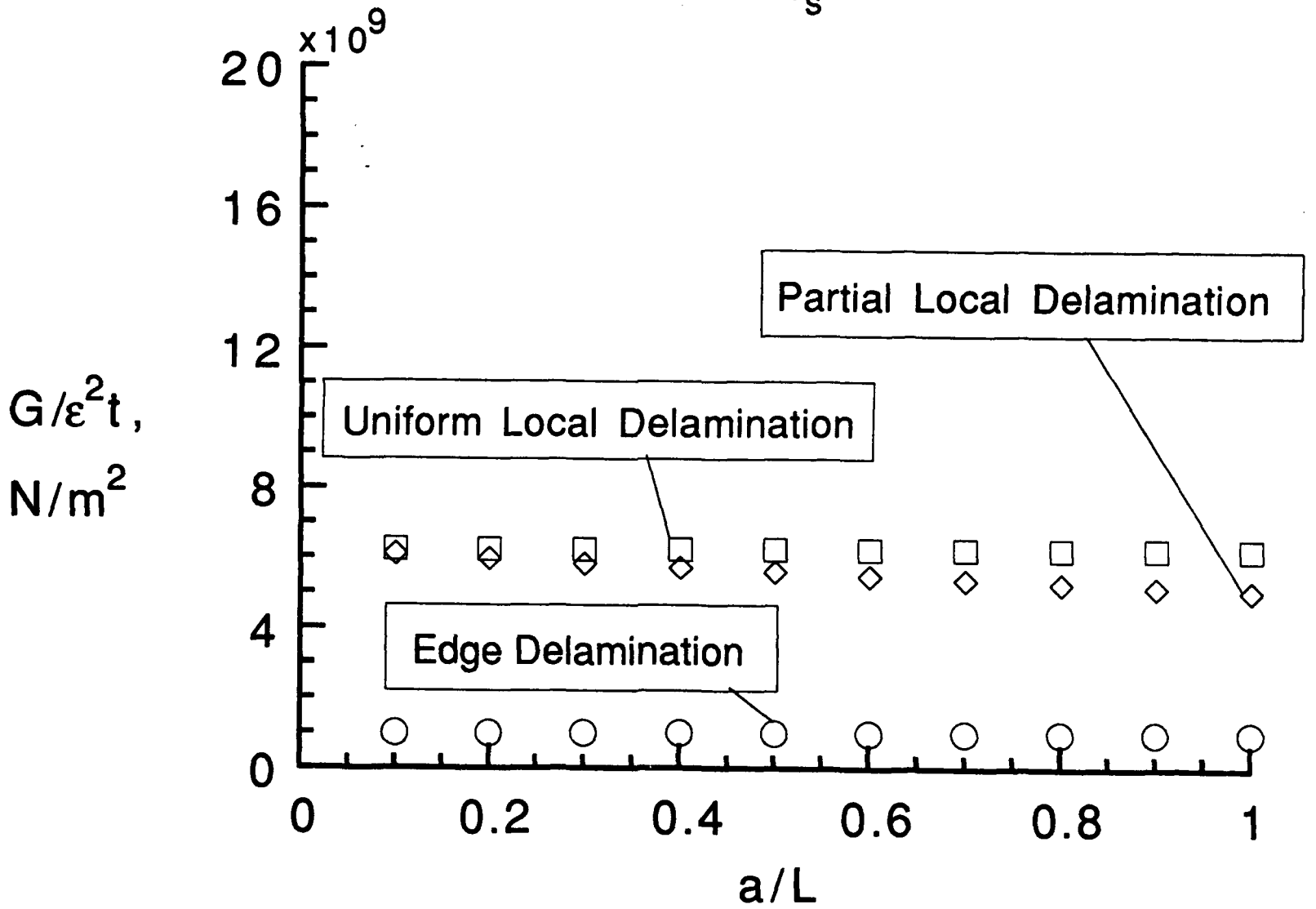

FIG.20 Normalized G for Local Delamination in θ/ -θ Interface of $(0/\theta/-\theta)_s$ Laminates

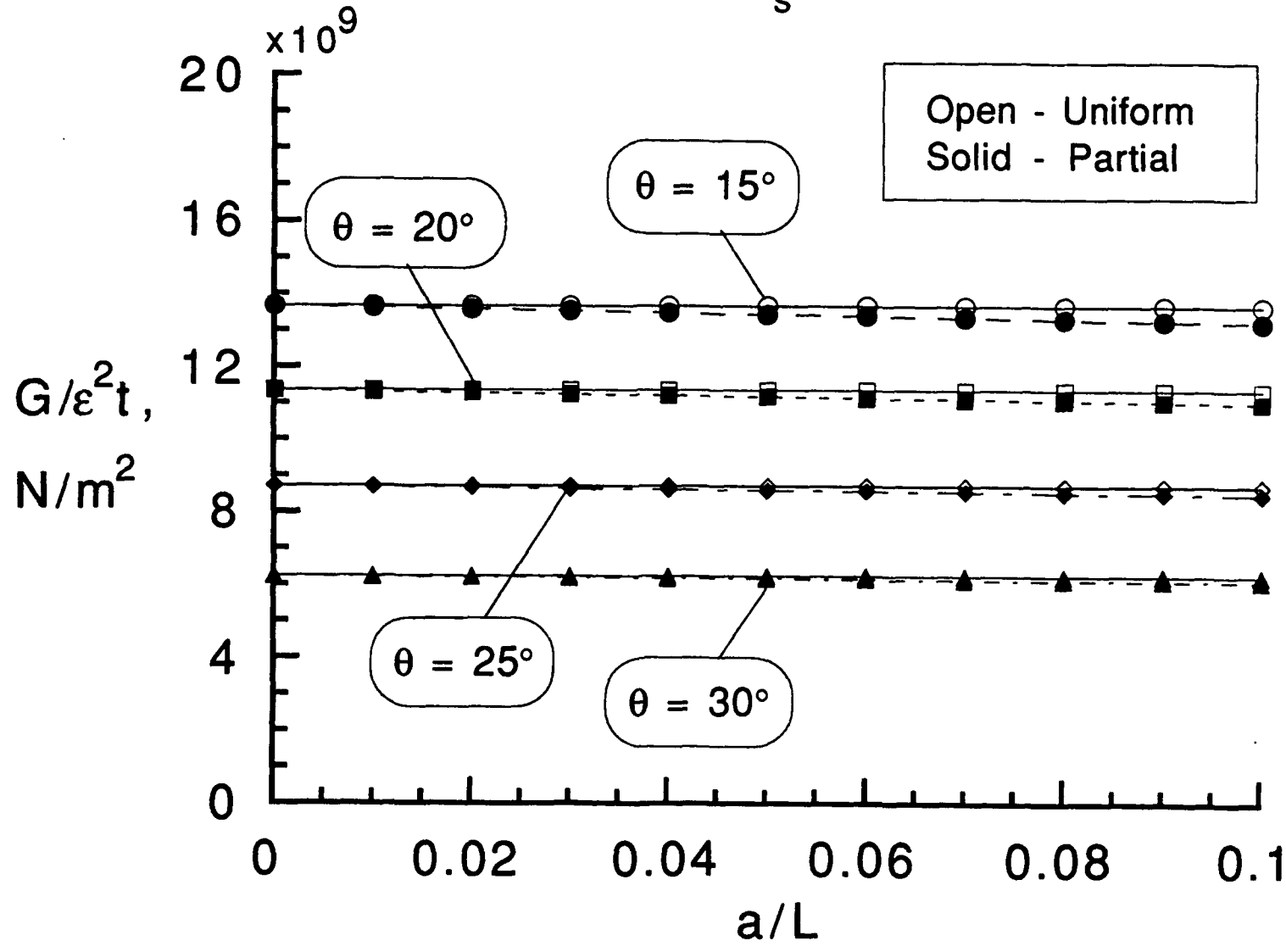

FIG.21 G^{M+T+H} FOR LOCAL DELAMINATION FROM -15 DEGREE MATRIX CRACK

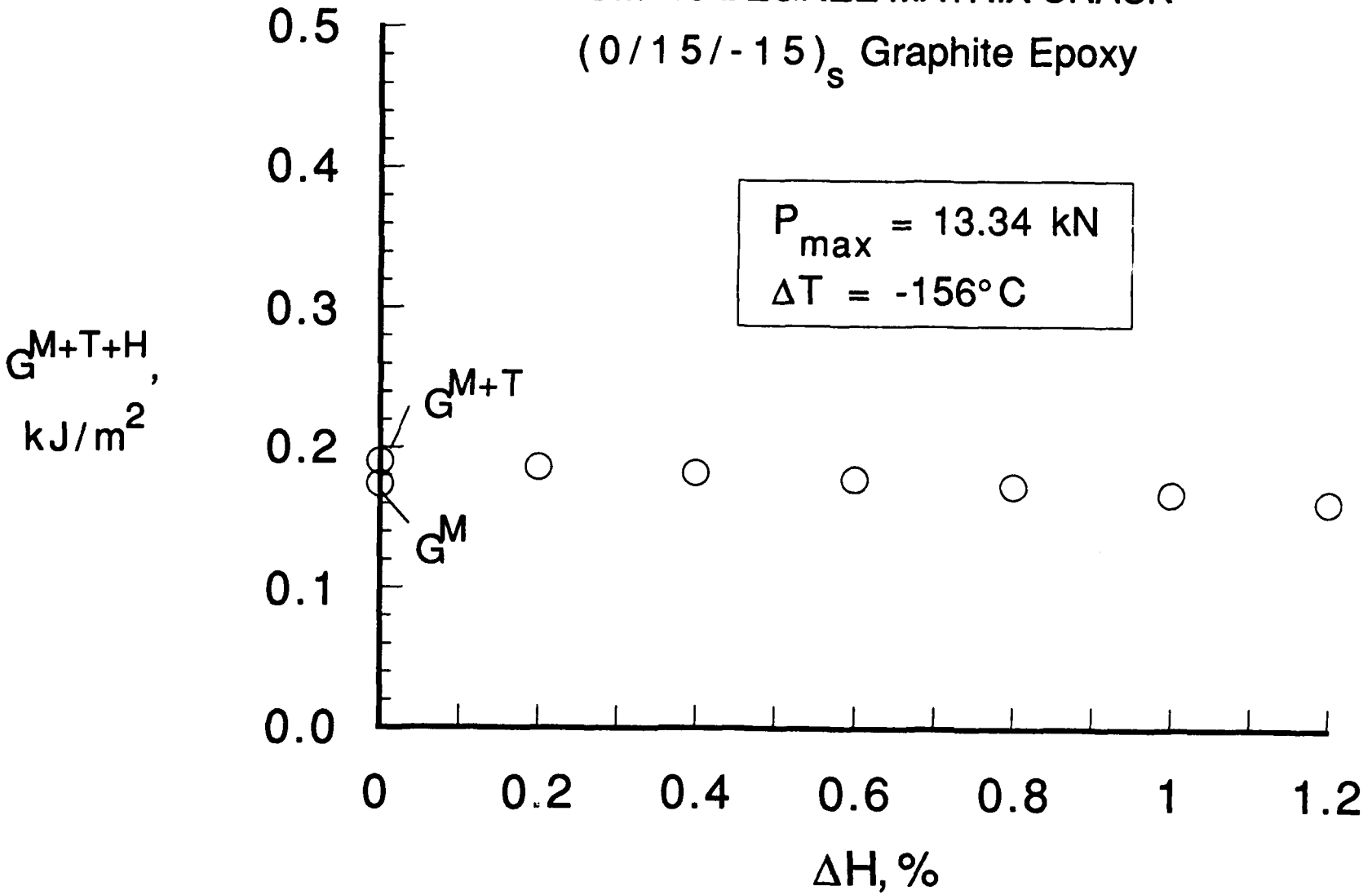

FIG.22 G^{M+T+H} FOR LOCAL DELAMINATION FROM -20 DEGREE MATRIX CRACK

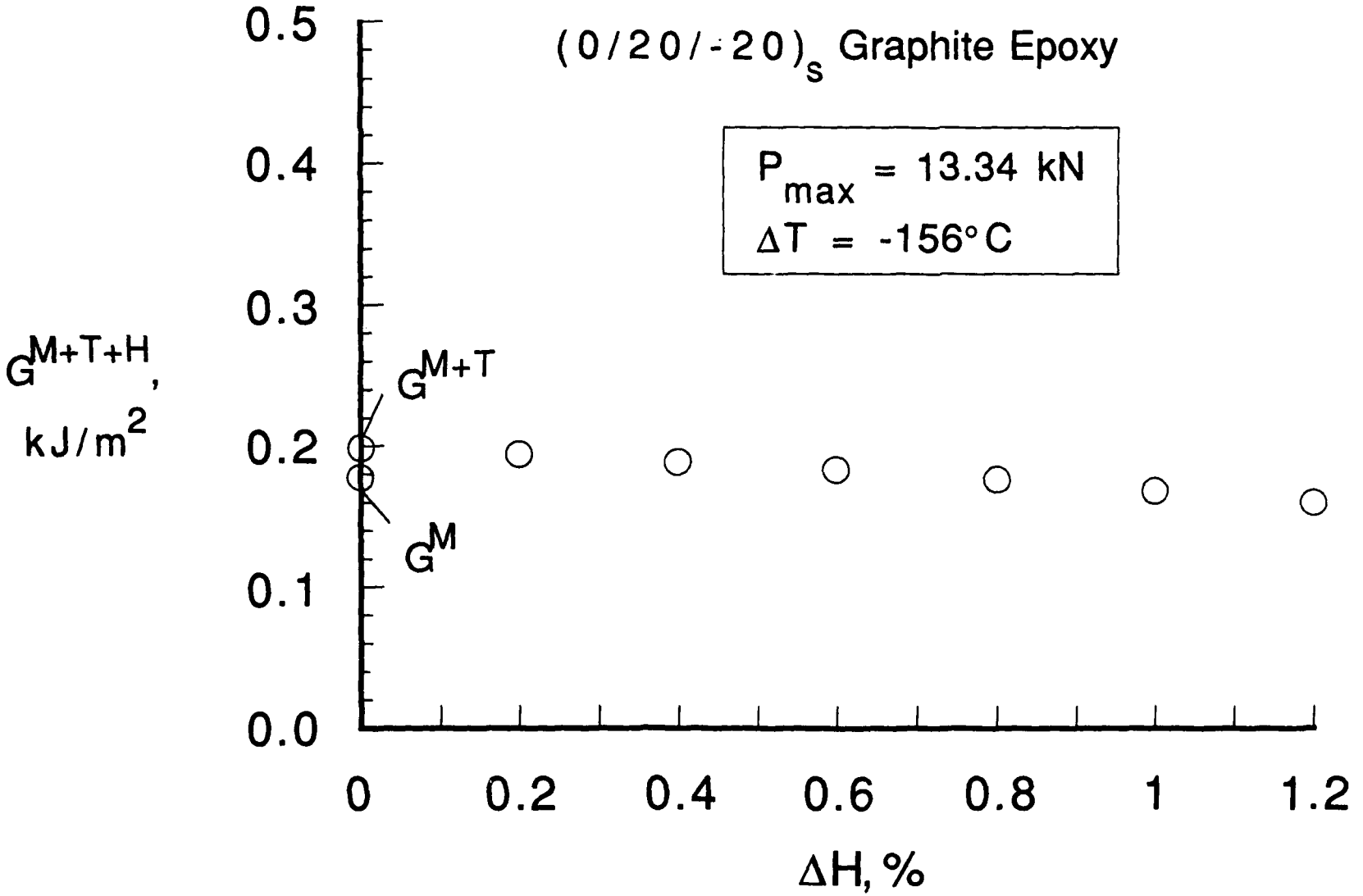

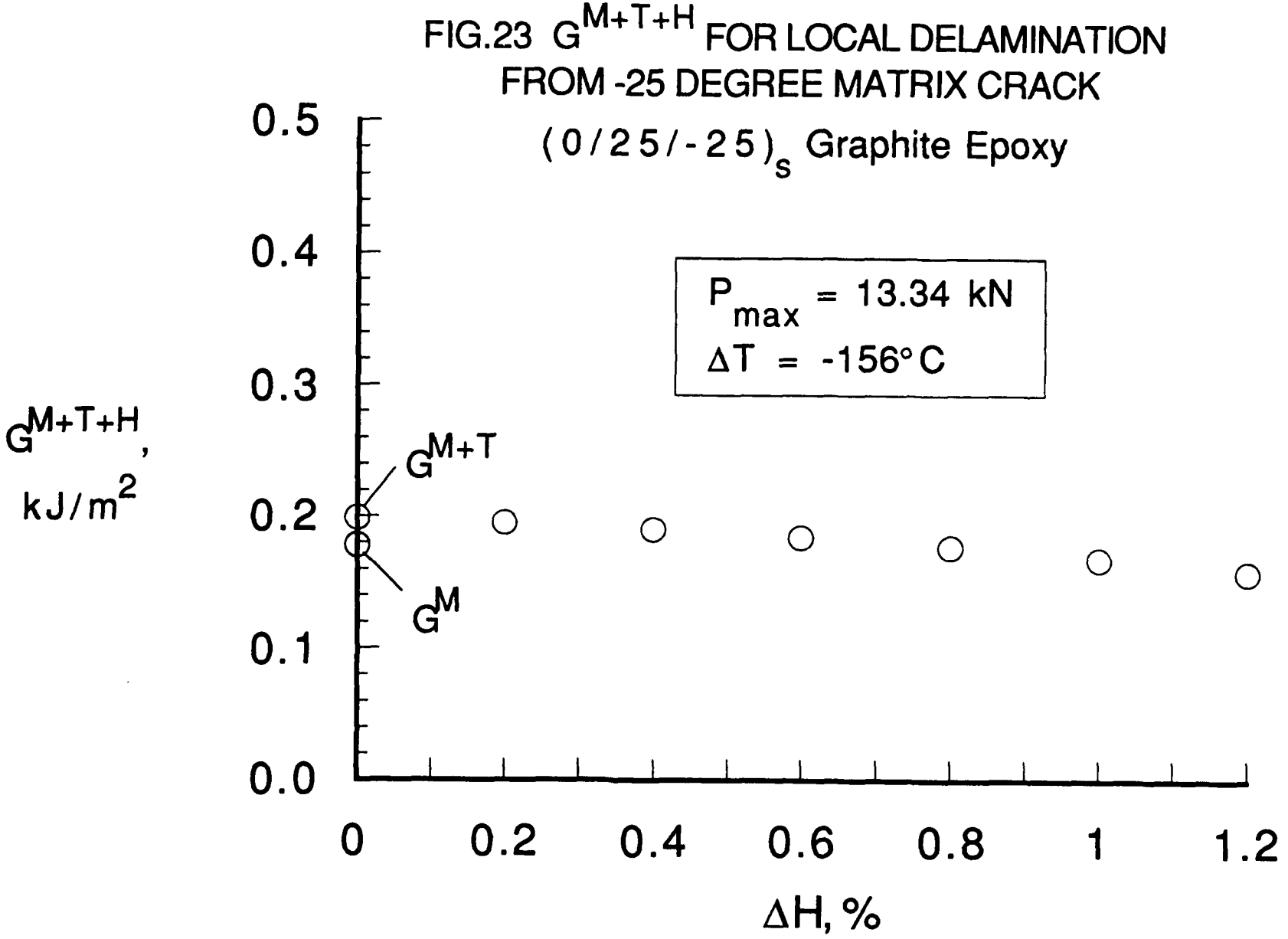
FIG.23 G^{M+T+H} FOR LOCAL DELAMINATION FROM -25 DEGREE MATRIX CRACK
$(0/25/-25)_s$ Graphite Epoxy
P_{max} = 13.34 kN
ΔT = -156°C
G^{M+T+H}, kJ/m²
G^{M+T}
G^{M}
0.5
0.4
0.3
0.2
0.1
0.0
0
0.2
0.4
0.6
0.8
1
1.2
ΔH, %

FIG.24 G^{M+T+H} FOR LOCAL DELAMINATION FROM -30 DEGREE MATRIX CRACK

$(0/30/-30)_s$ Graphite Epoxy

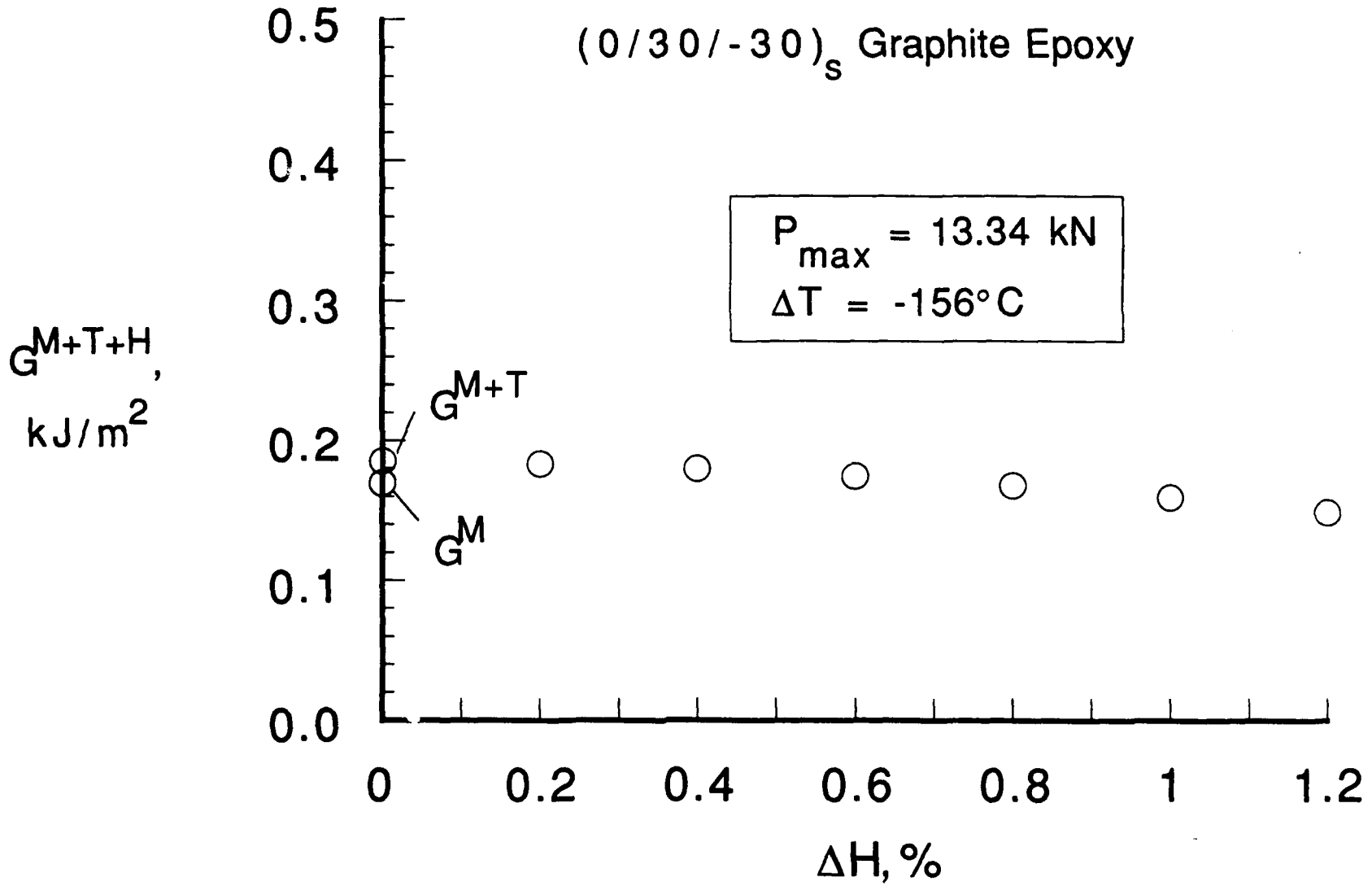

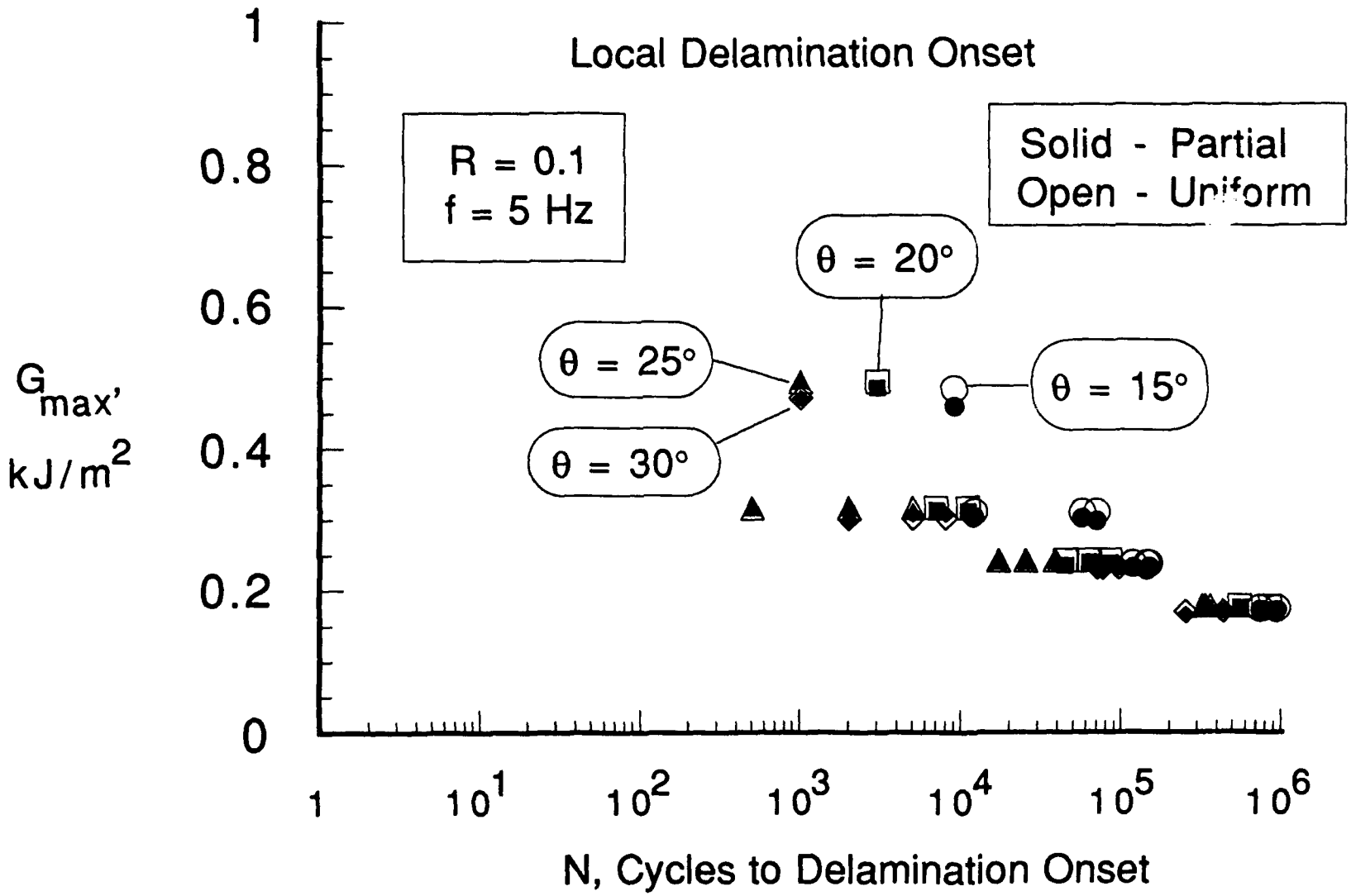
FIG.25 $(0_2/\theta_2/-\theta_2)_s$ AS4/3501-6
Local Delamination Onset
R = 0.1
f = 5 Hz
Solid - Partial
Open - Uniform
θ = 20°
θ = 25°
θ = 15°
θ = 30°
G_{max}, kJ/m^2
1
0.8
0.6
0.4
0.2
0
1
10^1
10^2
10^3
10^4
10^5
10^6
N, Cycles to Delamination Onset

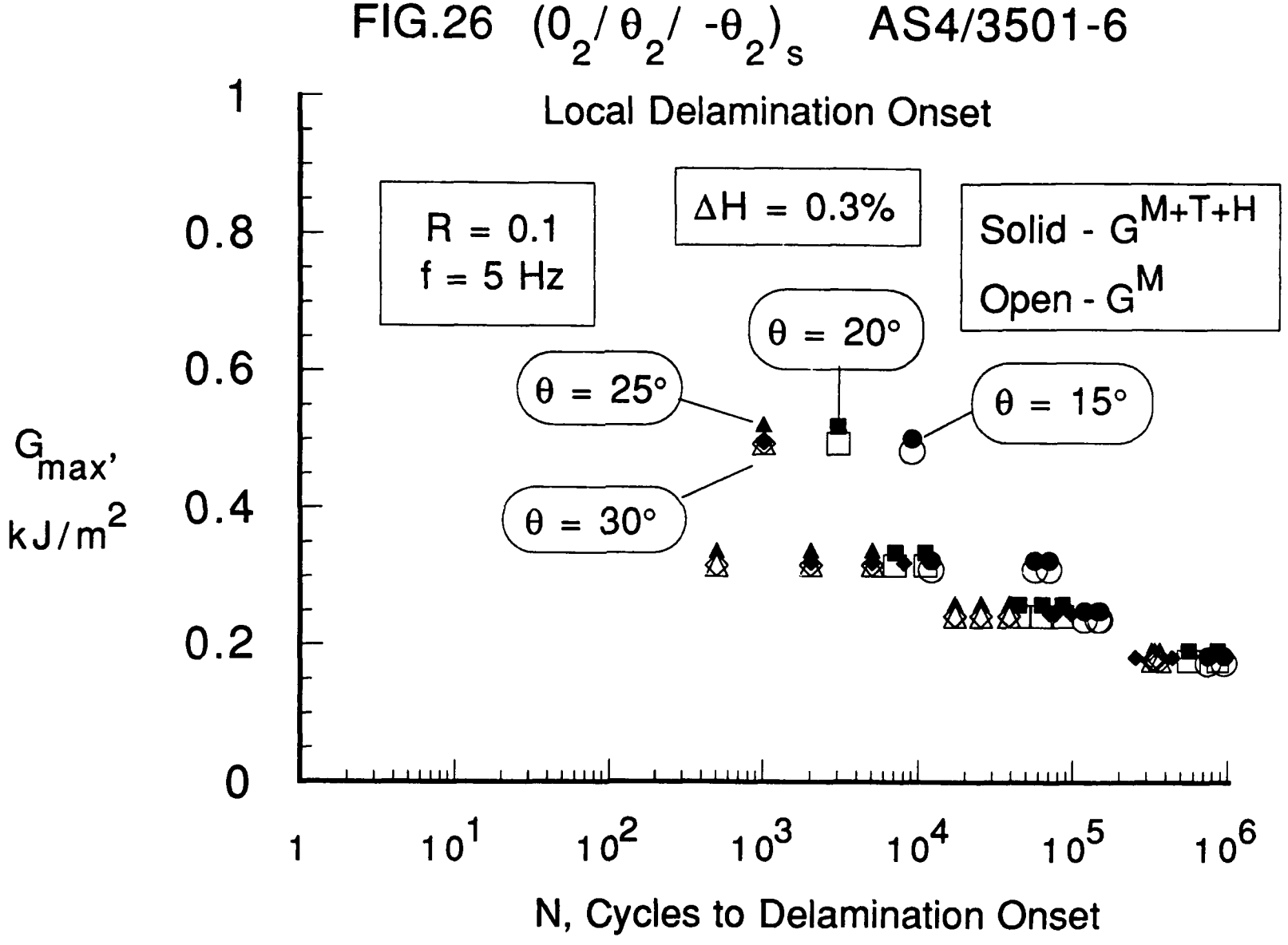
FIG.26 $(0_2/\theta_2/-\theta_2)_s$ AS4/3501-6
Local Delamination Onset
R = 0.1
f = 5 Hz
ΔH = 0.3%
Solid - G^{M+T+H}
Open - G^{M}
θ = 20°
θ = 25°
θ = 15°
θ = 30°
G_{max}, kJ/m^2
1
0.8
0.6
0.4
0.2
0
1
10^1
10^2
10^3
10^4
10^5
10^6
N, Cycles to Delamination Onset

FIG.27 $(0_2/\theta_2/-\theta_2)_s$ AS4/3501-6

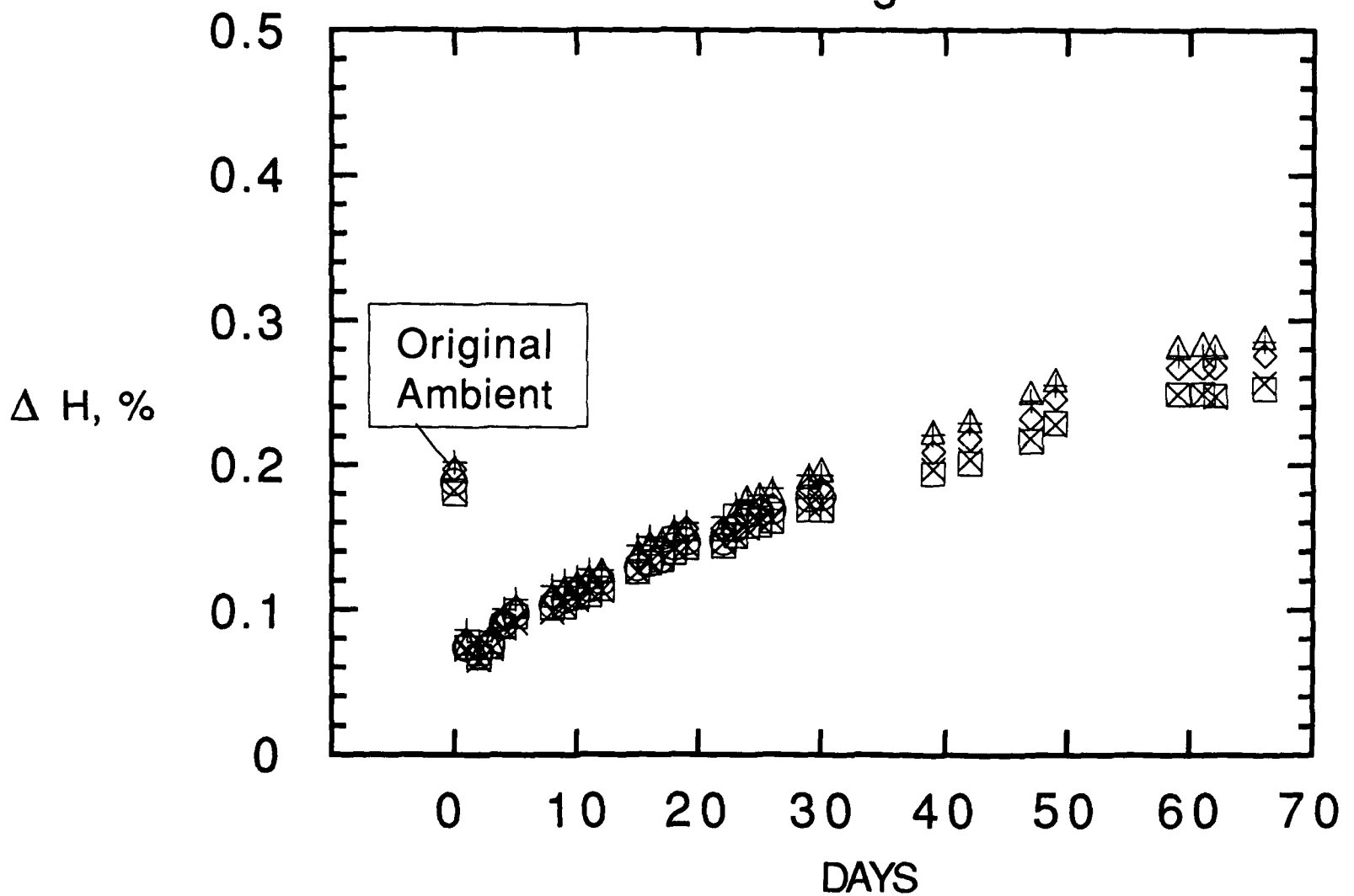

NASA

Report Documentation Page

1. Report No.	2. Government Accession No.	3. Recipient's Catalog No.
NASA TM-104076 AVSCOM TR-91-B-011		

4. Title and Subtitle	5. Report Date
Local Delamination in Laminates with Angle Ply Matrix Cracks: Part II Delamination Fracture Analysis and Fatigue Characterization	June 1991
	6. Performing Organization Code
7. Author(s) T. Kevin O'Brien	8. Performing Organization Report No.
	10. Work Unit No. 505-63-50-04
9. Performing Organization Name and Address NASA Langley Research Center, Hampton, VA 23665-5225 U.S. Army Aviation Research and Technology Activity (AVSCOM) Aerostructures Directorate Hampton, VA 23665-5225	11. Contract or Grant No.
	13. Type of Report and Period Covered Technical Memorandum
12. Sponsoring Agency Name and Address National Aeronautics and Space Administration Washington, DC 20546-0001 U.S. Army Aviation Systems Command St. Louis, MO 63166	14. Sponsoring Agency Code

15. Supplementary Notes

16. Abstract

Constant amplitude tension-tension fatigue tests were conducted on AS4/3501-6 graphite/epoxy $(02/\theta_2/-\theta_2)_S$ laminates, where θ was 15, 20, 25, or 30 degrees. Fatigue tests were conducted at a frequency of 5 Hz and an R-ratio of 0.1. Dye penetrant enhanced X-radiography was used to document the onset of matrix cracking in the central $-\theta$ degree plies, and the subsequent onset of local delaminations in the $\theta/-\theta$ interface at the intersection of the matrix cracks and the free edge, as a function of the number of fatigue cycles. Two strain energy release rate solutions for local delamination from matrix cracks were derived: one for a local delamination growing from an angle ply matrix crack with a uniform delamination growing from an angle ply matrix crack with a triangular shaped delamination area that extended only partially into the laminate width from the free edge. Plots of G_{max} vs. N were generated to assess the accuracy of these G solutions. The influence of residual thermal and moisture stresses on G were also quantified. However, a detailed analysis of the G components and a mixed-mode fatigue failure criterion for this material may be needed to predict the fatigue behavior of these laminates.

17. Key Words (Suggested by Author(s))	18. Distribution Statement
Composite material Graphite/epoxy Delamination Matrix crack Fatigue	Unclassified - Unlimited Subject Category - 24

19. Security Classif. (of this report)	20. Security Classif. (of this page)	21. No. of pages	22. Price
Unclassified	Unclassified	56	A04